THE ASTROPHYSICAL JOURNAL, 306:64–89, 1986 July 1

ON THE NATURE OF QSO HOST GALAXIES

ERIC P. SMITH[1] AND T. M. HECKMAN[1,2]
Astronomy Program, University of Maryland

G. D. BOTHUN[1]
Department of Astronomy, Caltech

W. ROMANISHIN
Physics Department, Arizona State University

AND

B. BALICK[1]
Department of Astronomy, University of Washington
Received 1985 August 12; accepted 1985 December 23

ABSTRACT

We present the results of an analysis of deep images of 31 low-redshift ($z \lesssim 0.3$) QSOs and lower luminosity QSO/AGNs obtained with the prime focus CCD system on the CTIO 4 m telescope. We have used two image-modeling programs to deconvolve the QSO from its host galaxy and thereby derive the absolute magnitudes, isophotal radii, and (in 12 cases) the morphological type (disk or elliptical) of the hosts. The derived absolute magnitudes of the hosts have been statistically corrected for the presence of spatially resolved emission-line nebulosity. Combining our data with other corrected data in the literature on 58 additional host galaxies yields the following results. First, we find that the host galaxies of QSOs are not drawn randomly from the general population of galaxies but are instead inhabitants of the "exponential tail" of the Schechter luminosity function. No plausible selection effects to explain this result have been uncovered, especially since unresolved QSOs constitute only $\sim 10\%$ of the sample. We interpret this result as implying that highly luminous (massive?) galaxies are particularly adept at hosting a QSO, or that the QSO phenomenon may be accompanied by a global "burst" of star formation. These interpretations have important implications for cosmic evolution of QSOs and galaxies and for the search for "dead QSOs" in galaxies at the present epoch. Second, we find that the radio-loud QSO host galaxies are ~ 0.7–0.8 mag more luminous on average than radio-quiet QSO hosts. A trend for elliptical (disk) models to be preferred for the radio-loud (radio-quiet) QSO and QSO/QGN hosts was also found. These results strengthen the basis for associating radio-loud (radio-quiet) QSOs with radio (Seyfert) galaxies. Third, we find that about half the QSOs and QSO/AGNs we have imaged are hosted by morphologically peculiar galaxies. These results suggest that galaxy interactions may be an important trigger of QSO activity.

Subject headings: galaxies: nuclei — galaxies: photometry — galaxies: structure — quasars — radio sources: galaxies

I. INTRODUCTION

Recent work on low-redshift ($z \lesssim 0.5$) QSOs has provided strong evidence that such objects are the highly luminous active nuclei of distant galaxies. Imaging observations (Wyckoff, Wehinger, and Gehren 1981; Hutchings, Crampton, and Campbell 1984, hereafter HCC; Gehren *et al.* 1984; Malkan 1984; Malkan, Margon, and Chanan 1984, hereafter MMC) have shown that the great majority of low-redshift QSOs are immersed in spatially resolvable nebulae ("fuzz") whose properties are consistent with those expected for galaxies at the cosmological distances inferred for the QSOs. Optical and radio spectroscopy of this "fuzz" has led to several detections of stellar absorption lines (Boroson and Oke 1984; Balick and Heckman 1983; Boroson, Oke, and Green 1982; Stockton and Mackenty 1983), and of H I $\lambda = 21$ cm emission (Bothun *et al.* 1984; Condon, Hutchings, and Gower 1985), all at the QSO redshift. Imaging data have also been used to show that low-redshift QSOs can be statistically associated with apparent companion galaxies (Yee and Green 1984), and this result has been explicitly confirmed by spectroscopy of many of these companions (Stockton 1982; Heckman *et al.* 1984).

"Environmental" studies of low-redshift QSOs like those summarized above may also prove crucial to efforts to determine how the QSO phenomenon is initiated in a galaxy nucleus, and why only a small fraction of QSOs are able to generate powerful radio sources. To a large extent, the search for environmental clues to these mysteries has been hampered by difficulty in extracting quantitative data on faint fuzz surrounding bright QSOs. The majority of the published images of low-redshift QSOs were acquired with photographic plates (which have notorious limitations in terms of the linearity and dynamic range that are so badly needed for a project of this kind). Accordingly, we have conducted a program of imaging of low-redshift QSOs which used a highly linear and efficient detector of large dynamic range (an RCA CCD), mounted on a large telescope (4 m) at an excellent site (CTIO) and have acquired deep exposures (limiting magnitude for stellar objects, $V \approx 25.5$–26) of 31 QSOs. The high quality of our data, and

[1] Visiting Astronomer, Cerro Tololo Inter-American Observatory, a facility of the NOAO, which is operated by AURA, Inc., under contract with the NSF.
[2] Also Department of Physics and Astronomy, The Johns Hopkins University.

our use of image-modeling programs, together allow us to reliably and quantitatively determine such properties as the absolute magnitudes, isophotal diameters, and (in some cases) the morphological types of the QSO host galaxies. We describe our observations and our analysis of the images in § II and discuss our results in § III (combining our data with published imaging data where appropriate). In § IV we consider the interpretation and implications of the observed distribution of the luminosity of QSO host galaxies, then summarize our principal conclusions in § V.

II. OBSERVATIONS AND DATA ANALYSIS

a) Observations

The images were obtained during four nights in 1983 October using the CCD camera at the prime focus of the 4 m CTIO reflector. The 352 × 512 pixel RCA chip with a 0".6 pixel^{-1} scale was used. Exposures, each of 30 minutes total integration, were taken in the V bandpass. Observing conditions were excellent and are listed for each of the imaged QSOs in Table 1. Conditions were photometric, and the seeing varied from 0".9 to 1".8 (FWHM). The typical rms noise levels in the sky background were $\sim$26.5–27.2V mag arcsec^2 after flat-fielding, and typical sky brightnesses were $\sim$21.3–$\sim$21.6V mag arcsec^{-2}. We were able to obtain useful data down to surface brightness levels of $\sim$27V mag arcsec^{-2} by azimuthally averaging pixels in the faint outer "fuzz" around each QSO. Images of our sample of QSOs are presented in Figure 1. The flat-fielding and defringing of the frames was carried out at the site. Standard star fields were observed two or three times a night.

b) Data Analysis

i) *Model Fitting*

We take the image of a QSO to consist of a composite of a nuclear point source (the QSO itself) and an underlying galaxy (the "host"), blurred by the point-spread function (PSF) of the imaging system (determined by the atmospheric seeing and instrumental focus). The essential problem then is that with the imaging data alone, the separation of the QSO from the host galaxy is unavoidably a model-dependent procedure. Even if the faint, outer portions of the fuzz are relatively uncontaminated by scattered QSO light, a galaxy model is needed to extrapolate back into the central regions of the image which are dominated by the QSO (i.e., the fractional contribution made by starlight to the pointlike central region of the image is not generally known *a priori*).

TABLE 1

BASIC OBSERVATIONAL DATA

Name	Redshift[a]	m_v(tot)[b]	FWHM Seeing[c]	Sky[d] (mag arcsec^{-2})	Noise[e] (mag arcsec^{-2})
0031−076	0.291	18.56	1".4	21.6	27.5
0037+061	0.063	16.77	1.6	21.4	27.1
0049+171 = Mrk 1148	0.064	15.62	1.5	21.4	26.7
0050+106 = I Zw 1	0.061	13.59	0.9	21.2	25.8
0105−008 (PKS)	0.316	17.51	1.1	21.3	26.9
0134+033 = PHL 1070	0.079	16.31	1.1	21.3	27.1
0135−057 = 4C −05.06	0.308	18.06	1.4	21.7	26.6
0137+012 (PKS)	0.260	17.23	1.0	21.2	27.0
0137−010 = UM 357	0.330	16.92	1.0	21.5	26.9
0146+089	0.270	17.02	1.0	21.1	26.4
0157+001 = Mrk 1014	0.164	15.09	1.1	21.5	26.3
0205+024 = Mrk 586	0.155	15.14	1.8	21.4	26.3
0213−484	0.168	16.96	1.1	21.5	27.1
0231+022 (PKS)	0.322	17.07	1.4	21.5	27.1
0530−379	0.290	16.47	1.2	21.6	27.0
0736+017 (PKS)	0.191	16.71	1.8	21.2	26.8
2130+099 = II Zw 136	0.061	14.42	1.6	21.5	26.6
2135−147 (PKS)	0.200	15.38	1.2	21.5	26.5
2141+175 (PKS)	0.213	15.62	1.1	21.4	26.8
2156−204	0.250	18.45	1.1	21.5	27.2
2209+185 (PG)	0.070	15.30	1.4	21.4	26.9
2214+139 = Mrk 304	0.067	14.70	1.0	21.5	26.6
2215−037	0.241	17.12	1.2	21.4	27.0
2233+135 (PG)	0.325	17.76	0.9	21.4	26.8
2247+140 (PKS)	0.237	16.48	1.2	21.4	26.7
2251+113 (PKS)	0.323	15.40	1.2	21.6	26.0
2300−189 (PKS)	0.129	16.71	1.2	21.4	27.3
2304+043 (PG)	0.042	15.02	0.9	21.6	26.9
2305+187 (PKS)	0.313	18.23	1.2	21.5	27.0
2328+167 (MC 3)	0.284	18.22	1.7	21.5	26.8
2355−082 (PKS)	0.211	16.84	1.4	21.6	27.4

[a] From Hewitt and Burbidge 1980 or Véron-Cetty and Véron 1984.

[b] Total V magnitude of the QSO plus fuzz, integrated out to a level of 28V mag arcsec^{-2} in surface brightness.

[c] Seeing in the CCD frame, directly determined from the bright (but unsaturated) stars used to construct the PSF used in the image modeling (see text).

[d] Mean sky brightness in the CCD frame.

[e] The rms noise level in the mean sky brightness. Averaging over large surface areas in the outer annuli of our QSO images allowed us to measure surface brightness $\sim$ 1.5 mag fainter than this.

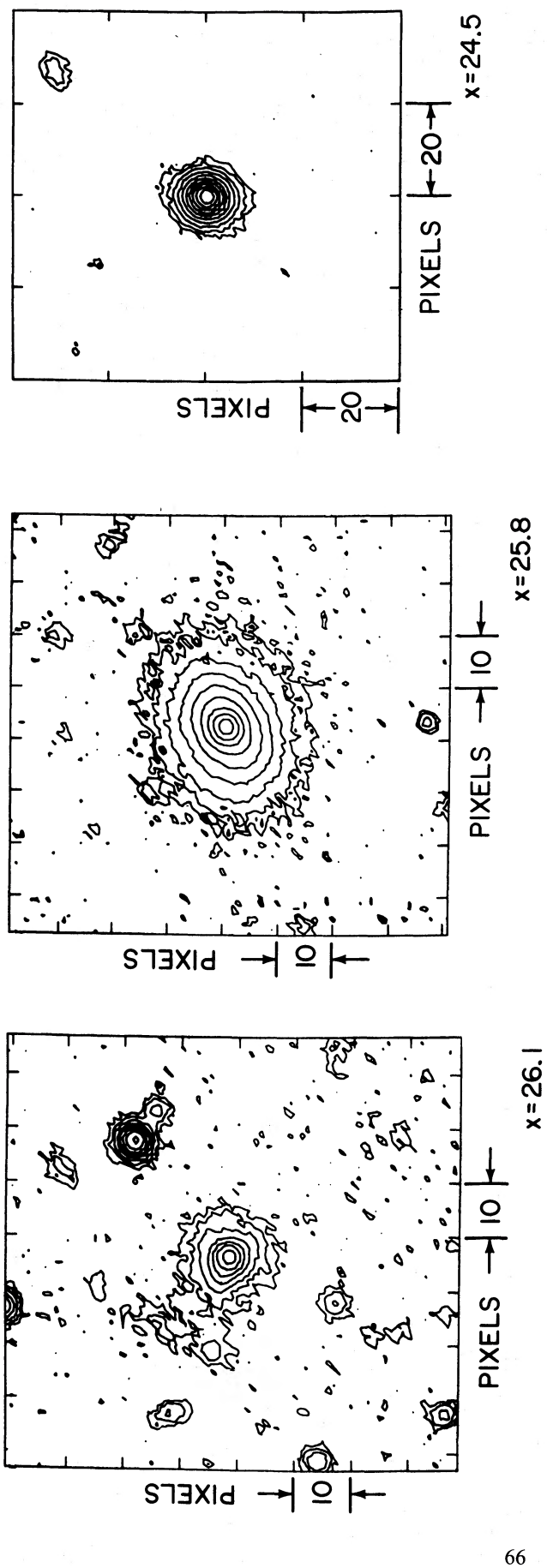

FIG. 1.—All images displayed with East up and North to the right. The value of x gives V mag arcsec^{-2} for faintest contour of image. Brightness profiles depict variation of surface brightness with distance (arcsec) from center of QSO (*plusses*). Point-spread function light distributions (*boxes*) have been scaled so that the intensity of the central pixel equals that of the QSO.

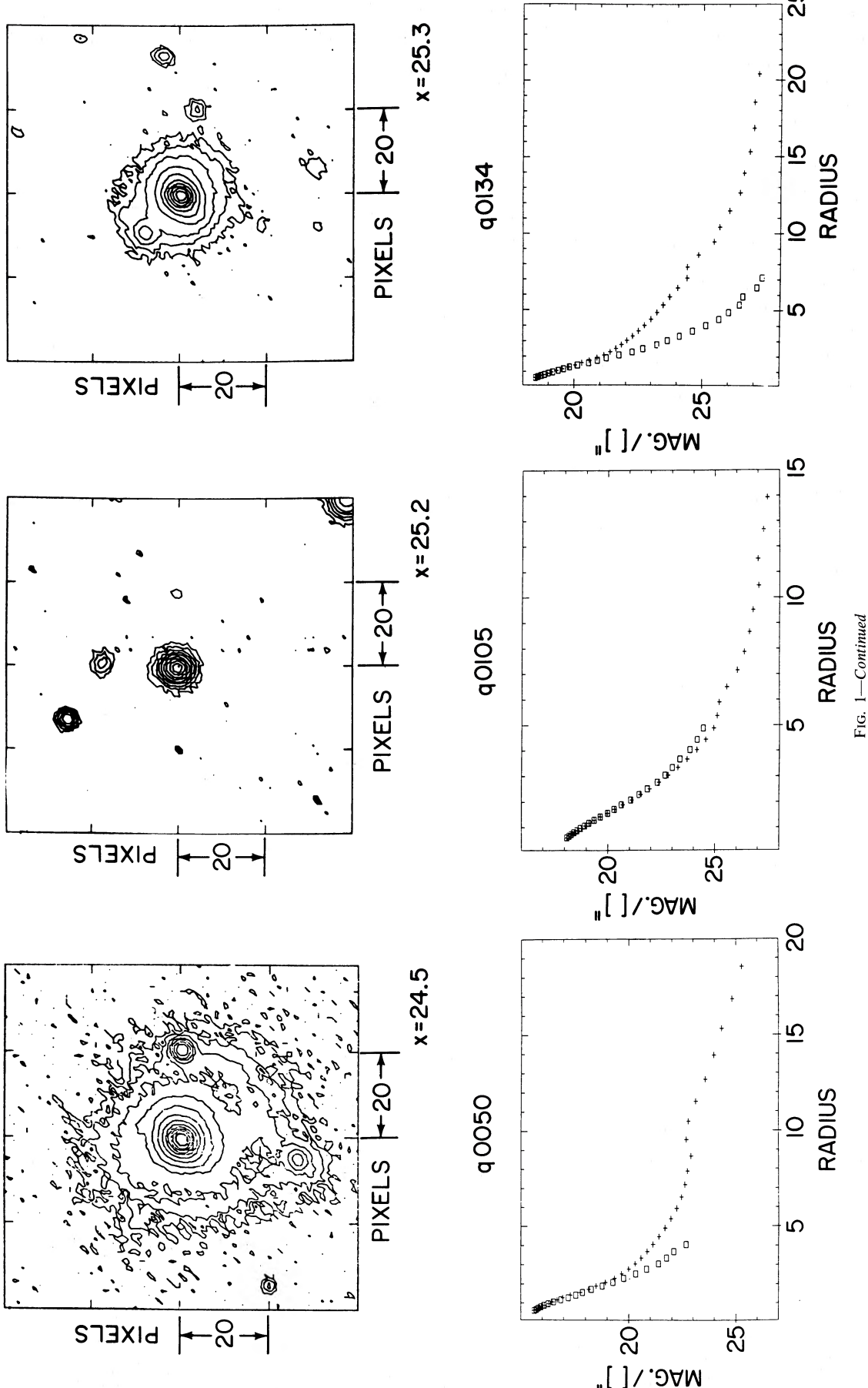

FIG. 1—*Continued*

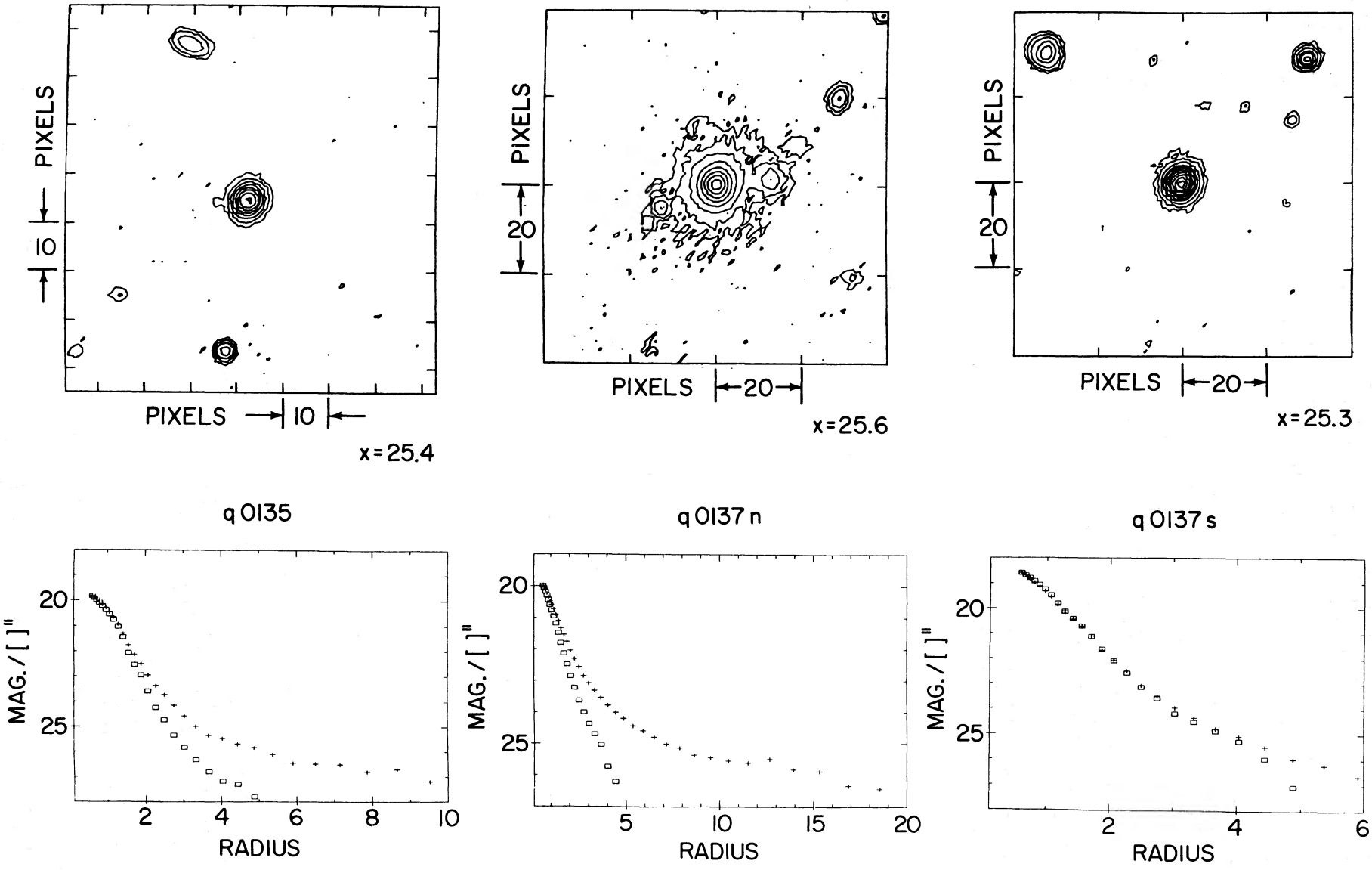

FIG. 1—*Continued*

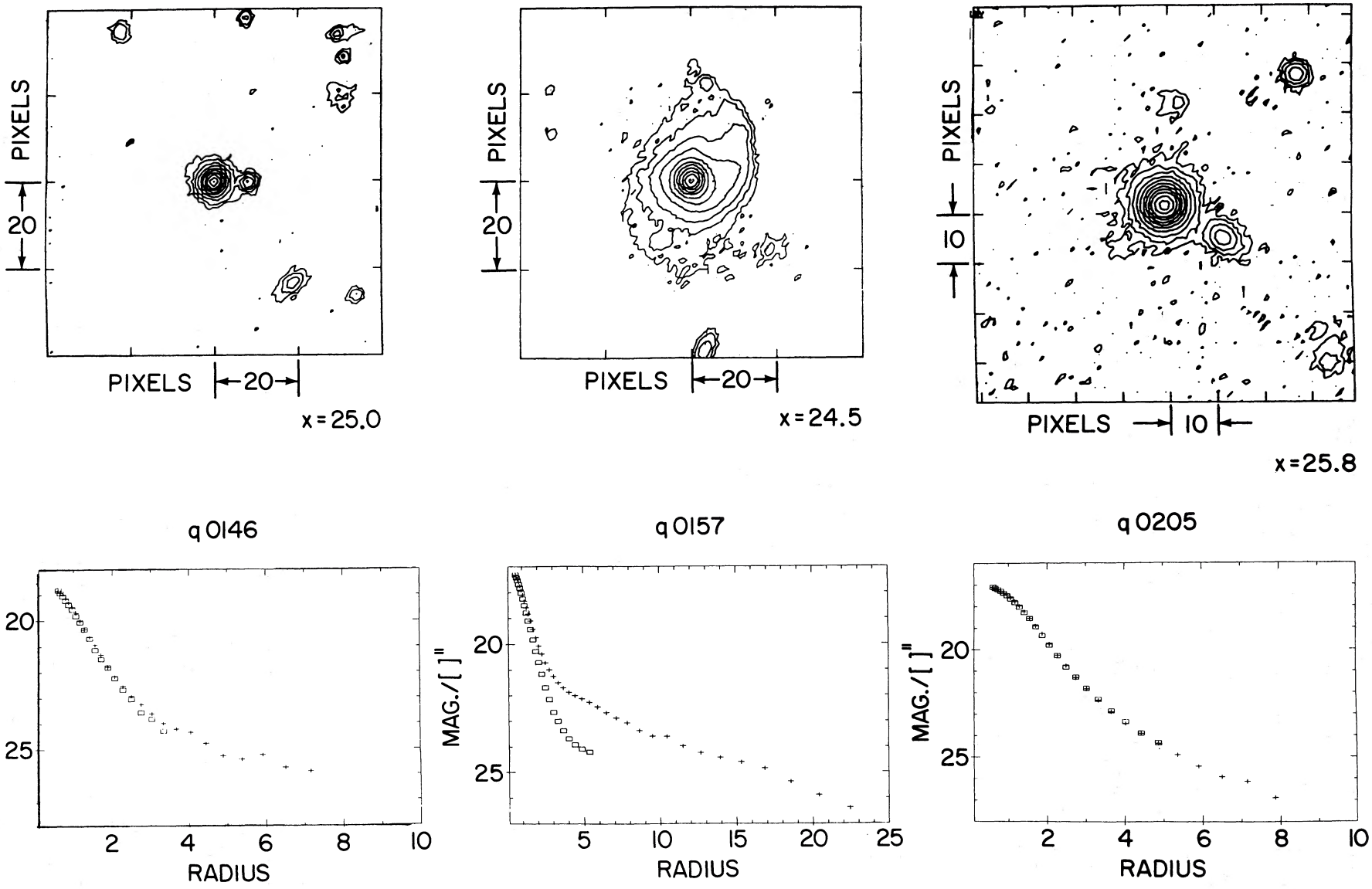

FIG. 1—*Continued*

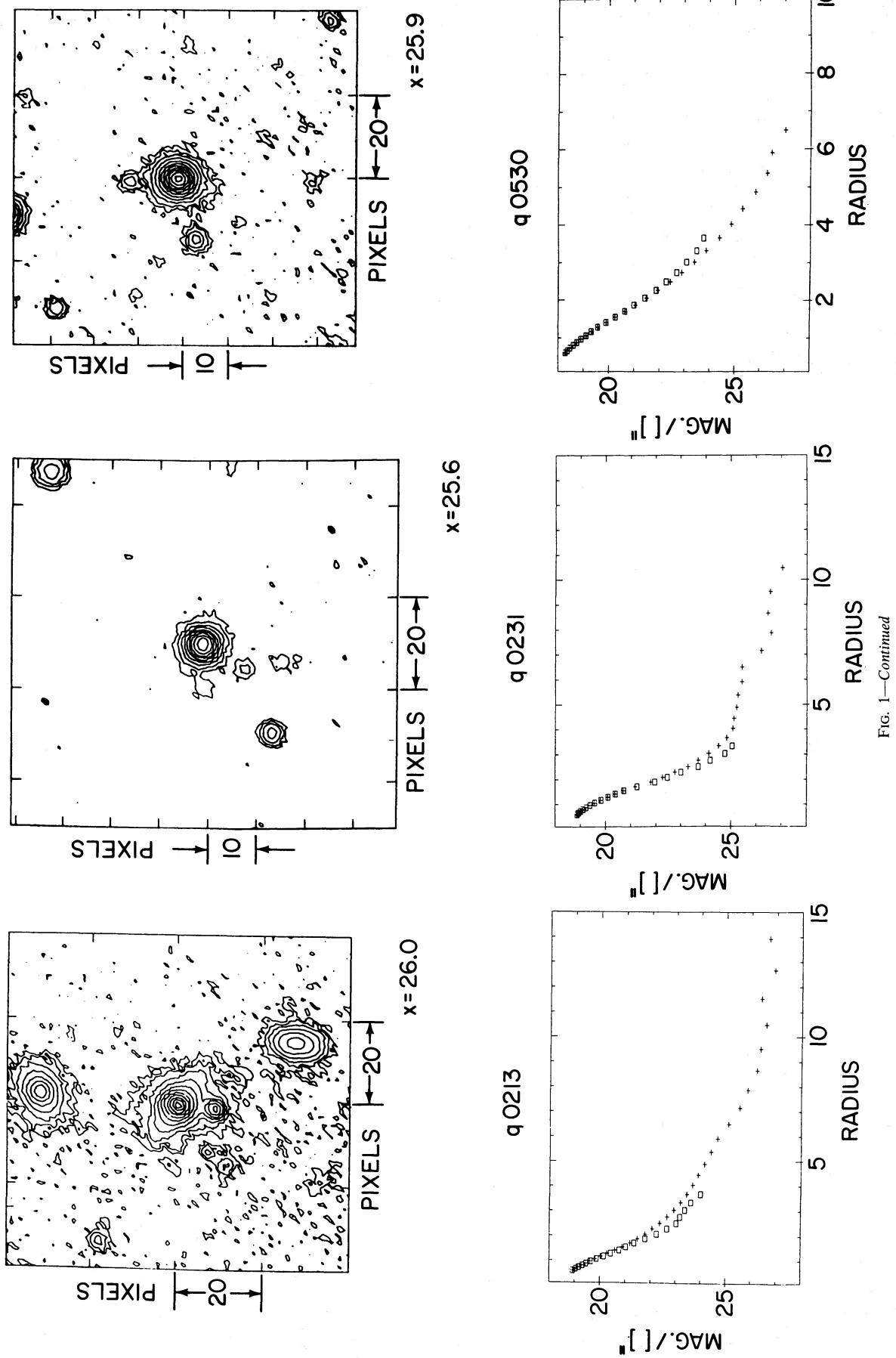

FIG. 1—*Continued*

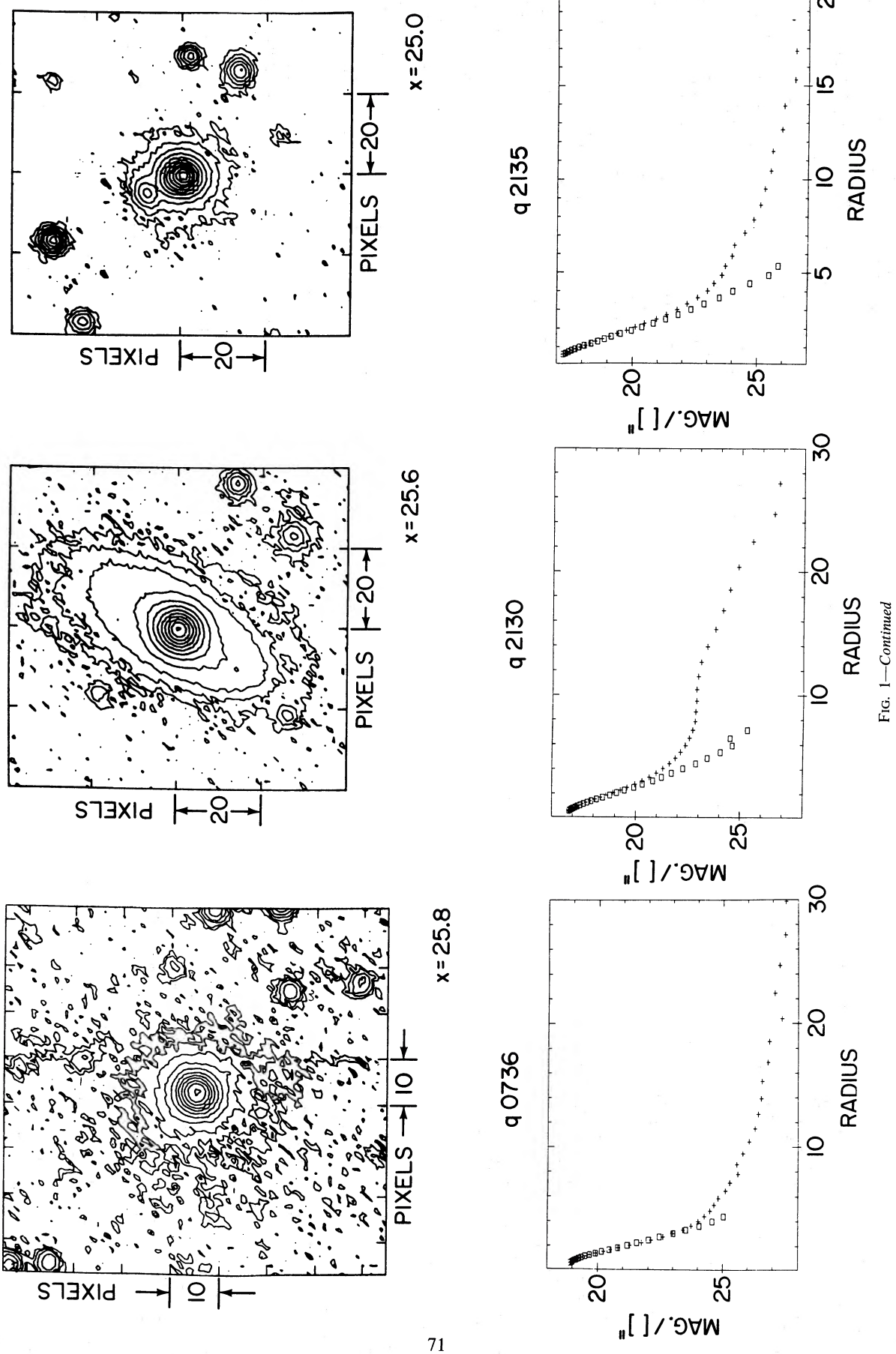

FIG. 1—*Continued*

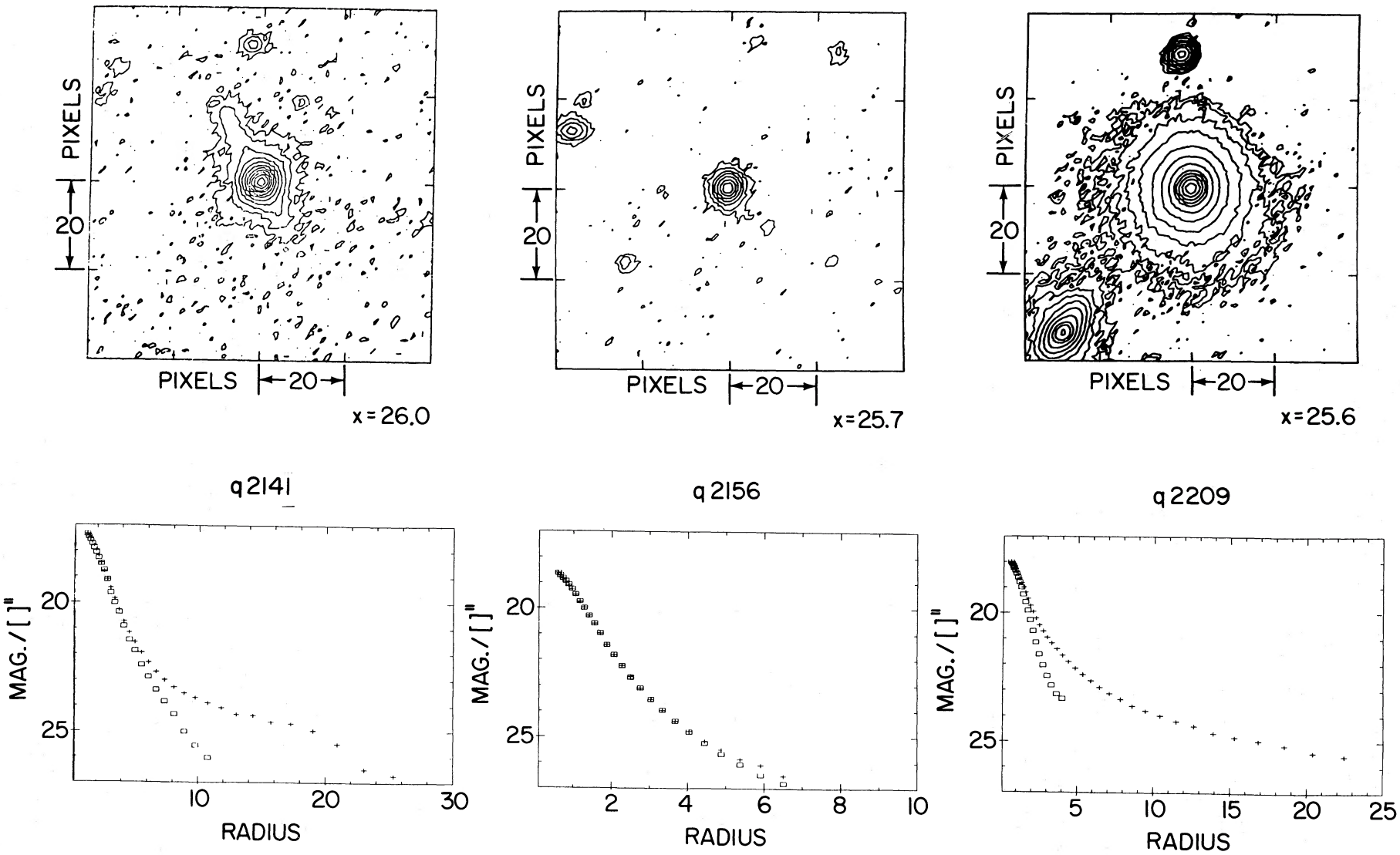

FIG. 1—*Continued*

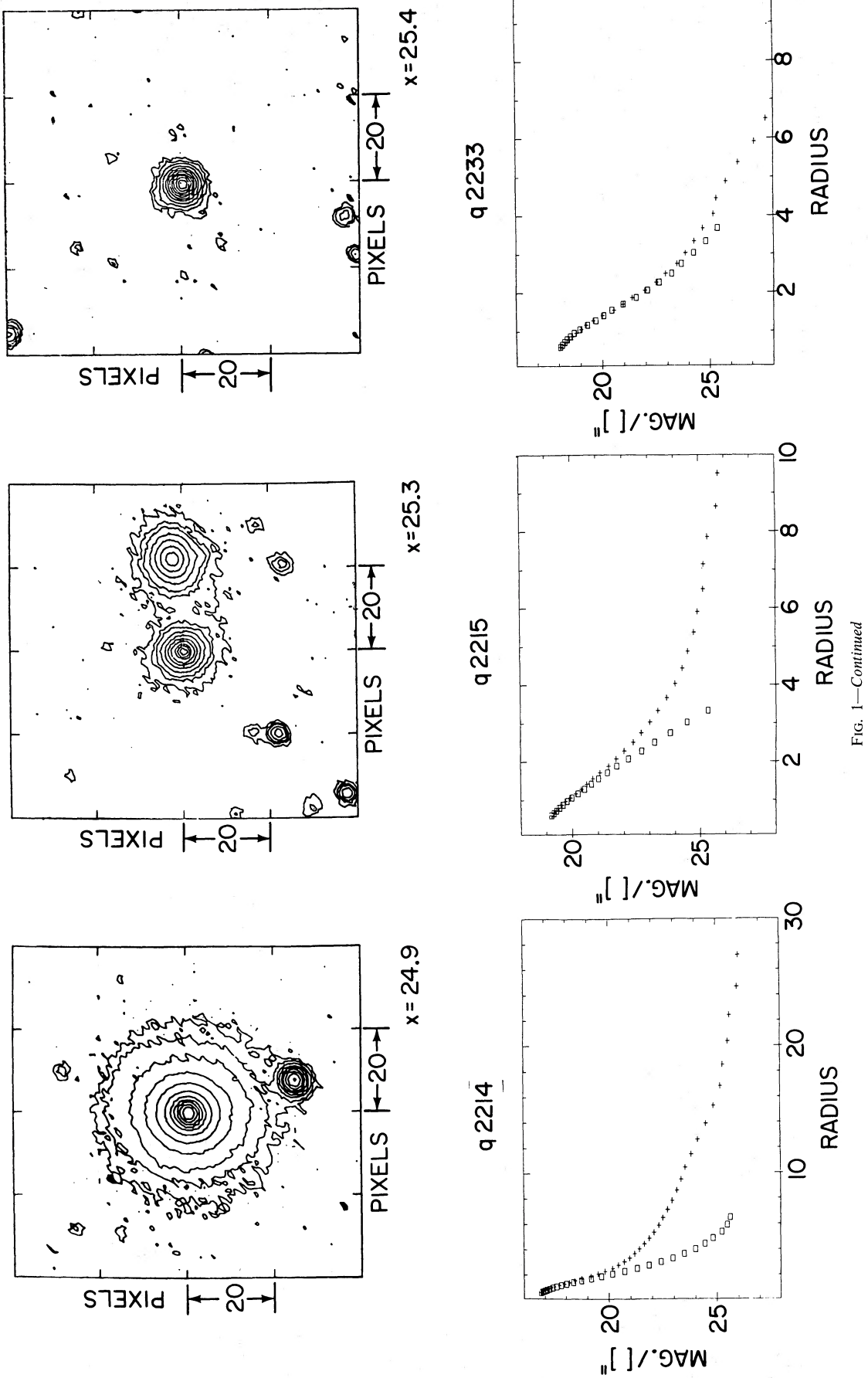

FIG. 1—*Continued*

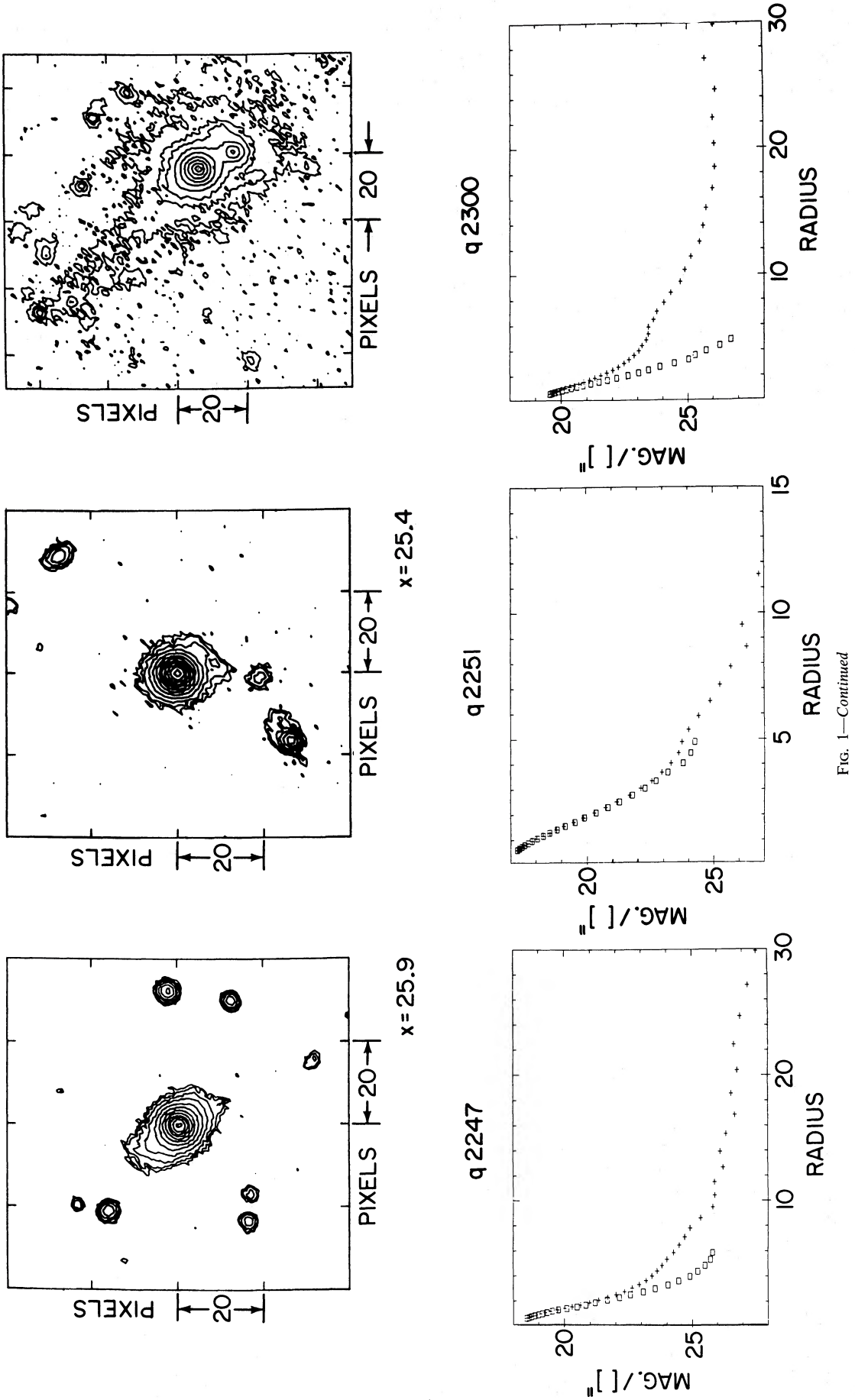

FIG. 1—*Continued*

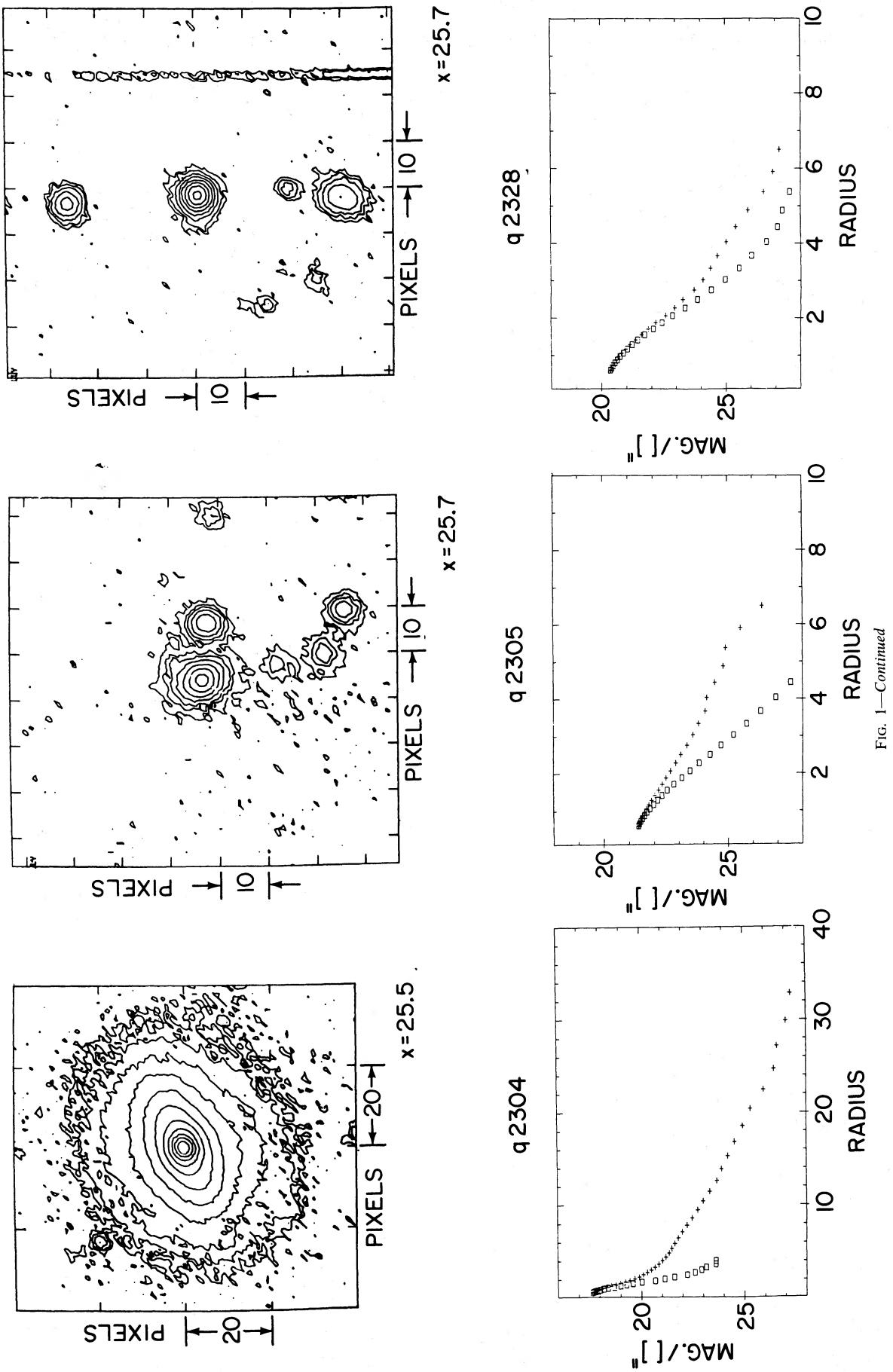

FIG. 1—*Continued*

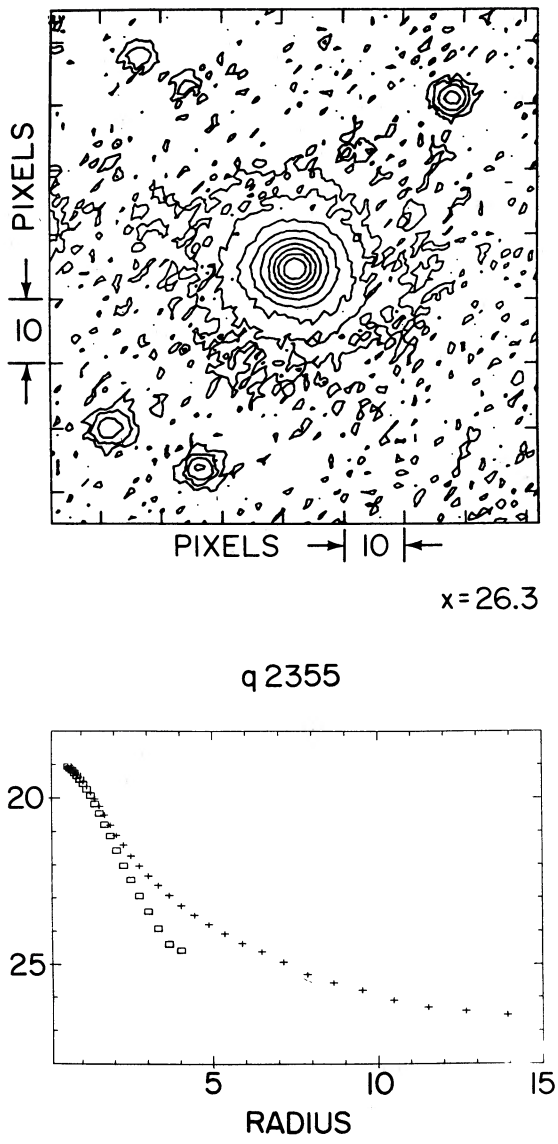

FIG. 1—*Continued*

Two of us (E. P. S. and G. D. B.) independently, using different image analysis packages, created computer models of galaxies plus point sources. The first package was written by one of us (W. R.) and is described in more detail in Romanishin *et al.* (1984) and Romanishin and Hintzen (1985). The second analysis was performed at Caltech (by G. D. B.) using a modified version of the GASP reduction package originally written by M. Cawson of Steward Observatory. In each case, the image of the QSO was first azimuthally averaged to produce a one-dimensional representation of the surface brightness profile. The azimuthal averaging could be done over elliptical rather than circular annuli, and the ellipticity and position angles of the elliptical annuli could be radially varied to match the properties of the "fuzz." Error bars for the image profiles were assigned by allowing for a ± 1 count sky subtraction error added in quadrature with the dispersion in the mean for each of the azimuthally averaged annuli. These errors, in counts, were then converted into the magnitude errors used by the model-building program. Error bars for annuli with radii less than 30 or so pixels (~ 8 pixels for stars) were ± 0.05 mag. The extreme wings of the profiles had errors which ranged typically from ± 0.2 to ± 0.5 mag. In the case of fuzz contaminated by stars or close companion galaxies or both, the azimuthal averages were done over the range(s) in position angle that excluded such contaminants. The azimuthally averaged PSF was explicitly determined for each frame in a like manner using a bright but unsaturated star (or, in many cases, the sum of two or more such stars) in the same frame as the QSO. In the cases where more than one star was used to create the PSF, it was found that the shape of the stellar profiles agree well. Variations of the PSF produced by changing seeing are implicitly account for by using the actual PSF data in our models. For the Romanishin package, no attempt was made at an analytical representation of the PSF. For the modified GASP package, the PSF was represented as the sum of two Gaussians (this functional form proved to be an excellent representation of the PSF). For both packages, the free parameters were:

1. The choice of disk (Freeman exponential) or elliptical (de Vaucouleurs $r^{1/4}$) galaxy models.
2. The relative flux of the QSO point source and the host galaxy (L_{PT}/L_{GAL}).
3. The galaxy scale length(s) (either the exponential scale length for the disk or the effective radius of the elliptical). In addition, disk models could be constructed with varying bulge/disk ratios.

Each model of galaxy plus QSO was convolved with the PSF appropriate to the image. The "blurred" model was then compared to the azimuthally averaged data, and a χ^2 value for the residuals computed. A series of such models was constructed for each QSO, and (following an iterative procedure) the grid in parameter space was made increasingly fine until a well-defined minimum in the χ^2 values was determined for each object. Disk galaxy models in the Romanishin package were constructed with bulge/disk ratios typical for Sa or Sb galaxies or both for many of the objects. QSOs modeled in this fashion yielded parameters for the underlying galaxy (scale length, L_{PT}/L_{GAL}) which were not significantly different from those generated by a point source plus a pure disk model. In 14 cases, acceptable fits could be obtained with both elliptical and disk galaxy models (we called these "multiply fit" images). In nine other cases, only a disk (or in three cases only an elliptical) galaxy model would produce an acceptable fit. Figure 2 is an example of an object with a radial brightness profile that could be modeled with an $r^{1/4}$ law galaxy but was inconsistent with an exponential disk model. Finally, for five cases, a pure QSO model produced the best fit, and only a lower limit to L_{PT}/L_{GAL} could be obtained. We regard our derived galaxy parameters as reliable only when the QSO image deviated from the PSF at levels of surface brightness $\mu_V < 23.5$ mag arcsec^{-2}.

For all these cases, we have defined an "acceptable fit" to mean that the value of χ^2 is such that the model *cannot* be rejected at the 95% confidence level when tested against the actual image. (It may be more clear to say that an "unacceptable" model is one which *can* be rejected at the 95% confidence level.) In Table 2 we list the best-fit values for L_{PT}/L_{GAL} for the fit and multiply fit images and appropriate upper limits for unresolved QSOs. We also give the corresponding ranges of L_{PT}/L_{GAL} which provided acceptable fits (for the well-resolved objects these correspond roughly to ± 2 σ limits). The χ^2 grid areas of acceptable fits defined roughly elliptical shapes, implying a correlation between model scale lengths and L_{PT}/L_{GAL} (see Table 2). The correlation spanned a larger region of parameter space for poorly resolved objects,

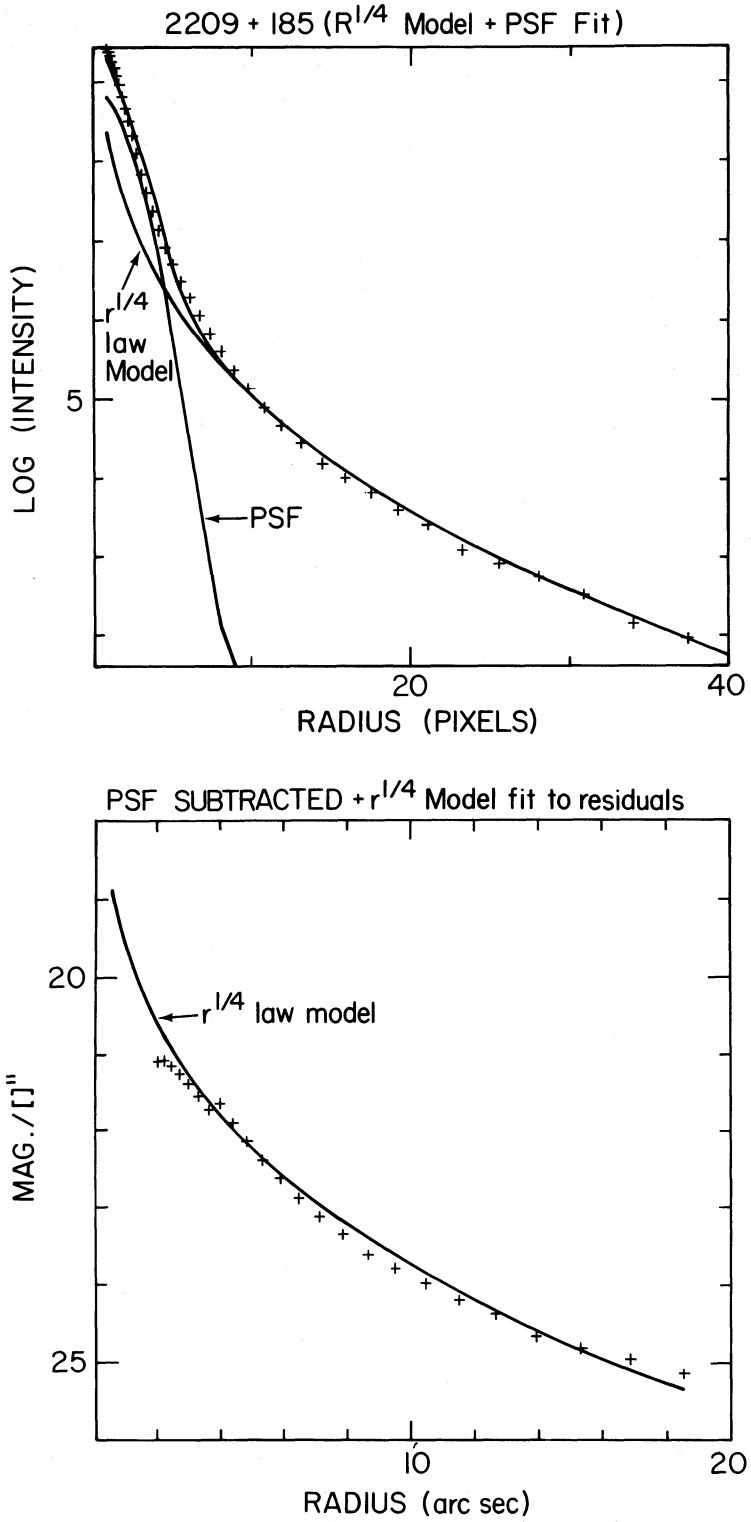

FIG. 2.—Two methods of modeling for 2209 + 185, an active nucleus hosted by an elliptical galaxy. (*a*) The result of adding a PSF to an $r^{1/4}$ law galaxy model and comparing this to the image profile, obtaining a best-fit model through minimization of χ^2. (*b*) Subtraction of the PSF first and fitting the residual galaxy with an $r^{1/4}$ law model. Obvious curvature of the image profile precludes a good fit by an exponential disk. Attempts to fit a disk also yield unrealistically low central surface brightness.

TABLE 2

DERIVED PARAMETERS

Name	Class	Model	Scale (kpc)	L_{pt}/L_{Gal}	R_{25}	M_B^{GAL}	M_B^{25}	M_B^{QSO}
0031-076	GLq	Disk	4.4±0.4	0.5+0.0 -0.1	17.4	-20.9	-20.8	-20.2
0037+061	GLq	Disk	2.1+0.2 -0.1	0.2+0.0 -0.1	7.4	-19.1	-19.3	-17.5
0049+171	QLq	E	2.9+2.2 -2.1	10.0+1.5 -5.0	4.8	-18.1	-18.8	-20.8
		Disk	2.1+2.1 -0.5	12.6+3.1 -2.9	5.0	-18.1	-18.6	-20.8
0050+106	QHq	Disk	3.1±0.4	3.4±0.6	13.9	-20.9	-20.4	-22.5
0105-008	QHl	E	...	15.9+ ∞ -9.6	(11.6)	-19.5	-20.3	-22.6
		Disk	...	15.9+ ∞ -9.6	(11.6)	-19.5	-20.1	-22.6
0134+033	QLq	Disk	2.3±0.4	1.6+0.1 -1.2	8.3	-19.3	-19.5	-20.1
0135-057	QHl	E	2.9+5.4 -1.9	1.3+1.2 -0.7	13.8	-21.0	-20.6	-21.4
		Disk	2.1+0.4 -0.0	3.6+1.4 -0.6	13.3	-20.3	-20.3	-21.8
0137+012	GLl	E	7.3±1.4	0.2±0.0	30.3	-21.9	-22.0	-20.7
0137-010	QHl		...	>10	...	>-21.2	...	-23.4
0146+089	QHq	(E)	2.1+4.7 -1.3	4.0+5.4 -2.5	17.6	-21.1	-21.1	-22.6
		Disk	5.6+5.5 -2.7	8.0+4.6 -3.0	17.0	-20.6	-20.7	-22.7
0157+001	QHq	Disk	10.8+0.6 -0.4	1.8+0.0 -0.1	30.4	-22.6	-21.8	-23.1
0205+024	QHQ		...	>20	...	>-19.6	...	-23.3
0213-484	QLq	Disk	3.9±0.1	3.0±0.0	12.5	-20.2	-20.2	-21.4
0231+022	QHl	E	9.9+5.6 -7.0	10.0+1.3 -4.0	21.3	-21.2	-21.4	-23.1
		Disk	8.8+4.4 -2.0	12.6+2.4 -4.1	20.9	-20.9	-21.1	-23.1
0530-379	QHq		...	>10	...	>-21.1	...	-23.5
0736+017	QHl	(Disk)	6.4±0.8	4.2+0.8 -0.0	14.9	-20.5	-20.5	-22.1
		E	8.7+2.6 -2.0	4.0+0.0 -0.8	15.1	-20.8	-20.8	-22.0
2130+099	QHq	Disk	4.5±0.2	4.2+0.1 -0.4	14.6	-20.4	-20.5	-21.7
2135-147	QHl	(Disk)	6.7+4.4 1.1	9.5+0.5 -2.0	18.9	-21.3	-20.9	-23.6
		E	5.9+4.1 -2.4	8.9+2.1 -1.8	21.5	-21.6	-21.4	-23.6
2141+175	QHl	Disk	6.6+4.3 -2.6	12.9+4.1 -1.7	22.9	-21.3	-21.3	-23.5
		E	2.9+8.6 -1.1	7.9±4.7	15.7	-20.9	-20.9	-23.5
2156-204	QLq		...	>25	...	>-18.0	...	-21.2
2209+185	GLq	E	2.8±0.7	0.3±0.0	11.1	-20.5	-20.3	-19.8
2214+139	QLq	Disk	3.7±0.4	1.2±0.1	12.5	-20.8	-20.2	-21.2
2215-037	QHq	E	3.3+2.0 -0.8	1.6+0.9 -0.4	18.9	-21.4	-21.2	-21.9
		Disk	4.9±0.7	2.7+0.2 -0.0	18.5	-21.0	-20.9	-22.1
2233+135	QHq		...	>25	...	>-19.1	...	-22.5
2247+140	QHl	Disk	9.8+4.0 -2.9	5.7+1.4 -1.2	21.4	-21.3	-21.1	-22.8
		E	6.1+0.6 -1.0	3.5+0.0 -0.3	21.7	-21.6	-21.4	-22.7
2251+113	QHl	E	2.7+0.0 -0.4	5.7+1.0 -0.5	24.0	-22.2	-21.6	-24.7
2300-189	GLl	E	5.6+1.0 -0.5	0.4+0.1 -0.0	14.8	-19.9	-20.8	-20.1
		Disk	6.0±2.0	0.3±0.1	16.5	-20.0	-20.7	-19.9
2304+043	GLq	Disk	2.6±0.2	0.4+0.1 -0.0	9.4	-19.9	-19.7	-19.2
2305+187	GLl	(E)	1.8+0.5 -0.3	0.1+0.3 -0.0	20.0	-21.7	-21.3	-19.3
		Disk	4.6±1.5	0.8±0.3	19.8	-21.4	-21.0	-21.0
2328+167	QLl	E	2.3+6.7 -0.9	2.5+1.5 -0.9	13.1	-20.4	-20.6	-21.3
		Disk	2.3+1.3 -0.0	0.9+5.4 -0.2	13.3	-20.9	-20.3	-20.9
2355-082	QHl	E	5.6+1.4 -0.8	1.1+0.1 -0.2	20.5	-21.7	-21.3	-21.7
		Disk	5.3±0.5	1.7±0.2	20.4	-21.3	-21.1	-21.9

while the more easily resolved objects yielded much smaller regions of acceptable fits. Note that the lower limits to L_{PT}/L_{GAL} for the five unresolved QSOs represent values that could be rejected at the 95% confidence level. In the case of 0105−008 we could not exclude a model of pure QSO at the 95% confidence level. It is a "marginally resolved" image.

We emphasize that in our galaxy modeling procedure the scale lengths and galaxy total fluxes were independently varied. Despite this, our best-fit galaxy models are astrophysically reasonable objects. In particular:

1. They obey well the same relation between isophotal radius (R_{25}) and absolute magnitude as do normal galaxies (see § II[ii]).

2. The central surface brightness of the model galaxy disks are close to the "canonical" value found for real disk galaxies [in the QSO rest frame we find a mean $B(0) = 21.3$ mag arcsec^{-2} with a standard deviation of 0.7 mag in our models].

3. The elliptical galaxy models obey (to within a factor of 2 in r_e) the relation between r_e and M_B exhibited by normal galaxies. We do not regard such factors of 2 as significant.

Further details concerning individual objects may be found in the Appendix.

ii) *Absolute Magnitudes*

From the average of our best-fit models, and using our photometric calibration, we obtained values for the apparent V magnitudes of each host galaxy and of each QSO. The absolute magnitude of each host galaxy was then calculated first by using the standard distance-luminosity relation for $q_0 = 0$ and $H_0 = 100$ km s^{-1} Mpc^{-1}:

$$M_V = m_v - 42.38 - 5 \log z(1 + z/2) - K(z) - A_v ,$$

where the foreground extinction A_v was taken from Burstein and Heiles (1982) and $K(z)$ was taken from Pence (1976) for Sab spirals and from Bruzual (1983*a*) for ellipticals (his $\mu = 0.7$ model). The V magnitude was then converted into an absolute B magnitude using the data of Pence or the model of Bruzual to construct a rest-frame $B-V$ color for the appropriate galaxy type. This procedure makes our derived absolute B magnitude rather insensitive to the true spectral energy distribution of the galaxy, since for the typical redshifts of our sample of QSOs the spectral region observed through our V filter roughly corresponds to that measured by a B filter in the QSO rest frame. To facilitate comparison of our data to data on normal galaxies, the calculated M_B include only the light contained within the region of the galaxy where the surface brightness is 25B mag arcsec^{-2} or greater (in the quasar rest frame).[3] The calculated host galaxy magnitudes from each of the two independent analyses agreed well with $|\Delta M_B| = 0.20$ and $|M_B(\text{E. P. S.})| - |M_B(\text{G. D. B.})| = -0.02 \pm 0.06$.

For computation of a QSO absolute magnitude, a similar procedure was followed except that we have taken $B-V \approx 0$ for the QSO light. The crudeness of this procedure is justified, since the true spectral energy distributions of the QSOs in our sample are largely unknown, and because very accurate QSO absolute magnitudes are not germane to our purposes.

As a second, less direct method for calculating the host galaxy absolute magnitude we have used the average R_{25} isophotal radii of the host galaxies—from both model-fitting procedures—measured at the level of $B = 25$ mag arcsec^{-2} in the QSO rest frame, and the well-defined relations between R_{25} and M_B for normal galaxies.[4] This method is not completely independent of the first, more direct methods discussed above, since in all cases the same galaxy model was used to determine (and remove) the effects of the QSO light. The second method is, however, largely independent of the first, since there was no attempt made in the fitting procedure to use galaxy models which obeyed any specific relationship between absolute mag-

[3] We take the relationship between b_V (the observed surface brightness at V) and b_B^* (the surface brightness at B in the rest frame) to be given by

$$b_V = [b_B^* - (B-V)^*]10^{-0.4K(z)}/(1+z)^4 ,$$

where b_V and b_B^* are measured in mag arcsec^{-2}, $(B-V)^*$ is the QSO rest frame $B-V$ color of the outer part of the host galaxy (taken to be 0.9 for ellipticals and 0.6 for spirals), and $K(z)$ is the K-correction appropriate to the same regions. $K(z)$ was taken from Pence (1976) for spirals and from Bruzual's (1983*b*) $\mu = 0.7$ models for ellipticals. We convert angular to linear scales via the appropriate relation for $H_0 = 100$ km s^{-1} Mpc^{-1} and $q_0 = 0$:

$$r(\text{kpc}) = 14.54(z + z^2/2)/(1+z)^2\theta \text{ (arcsec)} .$$

[4] We use $\log R_{25}(\text{kpc}) = -3.87 - 0.246M_B$ for spirals, from Rubin (1983) adjusted to $H_0 = 100$ km s^{-1} Mpc^{-1}. Holmberg's (1975) work showed that the M_B vs. $\log R_{26.5}$ relations for ellipticals and spirals had the same slope, but the ellipticals were systematically $\sim$0.3 mag brighter for a given isophotal radius. Hence, we adopt $\log R_{25}(\text{kpc}) = -3.94 - 0.246M_B$ for ellipticals.

NOTES TO TABLE 2

Class.—The first classifying letter denotes image dominated by either the galaxy (G) or QSO (Q) according to whether or not $L_{PT}/L_{GAL} < 1$. The second classifying letter indicates whether QSO optical luminosity is higher (H) or lower (L) than the fiducial value $M_B = -21.5$ (Schmidt and Green 1983; Véron-Cetty and Véron 1984) which is appropriate to our choice of $H_0 = 100$ km s^{-1} Mpc^{-1}. The third letter indicates radio-loud (l) or radio-quiet (q) based on the ratio of the QSO optical to radio brightness relative to a fiducial value of the effective optical to radio spectral index $\alpha_R^O = 0.40$ (see text).

Model.—Type of galaxy model employed (disk or elliptical). In some cases, acceptable fits could be made with both elliptical and disk galaxy models. In other cases, only a disk or an elliptical model produced an acceptable fit. For unresolved QSOs, no type is given. Astrophysically suspect models given in parentheses. See Appendix.

Scale.—Length scale for the model galaxy. This was either the effective radius r_e for the elliptical galaxies or the Freeman exponential surface-brightness scale length r_0 for the disk galaxies. Values beyond the quoted limits represent models which can be rejected at the 95% confidence level. No values are given for unresolved or marginally resolved images.

L_{PT}/L_{GAL}.—Ratio of the total flux in the V filter from the point (QSO) and galaxy components in our best-fit models. Values beyond the quoted limits represent models which can be rejected at the 95% confidence level. Upper limits for unresolved QSOs imply that models with lower values of L_{PT}/L_{GAL} can be rejected at 95% confidence level. For two marginally resolved QSOs, the upper limit on L_{PT}/L_{GAL} extends formally to infinity.

R_{25}.—The average isophotal radius in kpc of the host galaxy ($H_0 = 100$ km s^{-1}, $q_0 = 0$). This is measured at an isophotal level of 25B mag arcsec^{-2} in the QSO rest frame. The best-fit models have been used to subtract scattered QSO light, but R_{25} is directly measured form the "QSO-less" images (not determined from the model).

M_B^{GAL}.—The average absolute blue magnitude of the host galaxy derived from the best-fit models. This has been calculated as described in the text.

M_B^{25}.—The absolute blue magnitude of the host galaxy derived from the directly measured R_{25} and the assumption that QSO host galaxies obey the same relations between R_{25} and M_B as normal spirals and ellipticals (see text).

M_B^{QSO}.—The absolute blue magnitude of the QSO alone (no galaxy contribution) as derived from the best-fit model. See text.

nitude and isophotal radius. We regard the good agreement between M_B obtained by the two methods ($|M_B^1 - M_B^2| = 0.25 \pm 0.04$ mag.; $M_B^1 - M_B^2 = -0.09 \pm 0.06$ mag) to be evidence that our model-fitting procedures were reliable.

iii) *Correction for Emission Lines in Fuzz*

Recent long-slit spectroscopic (Boroson, Persson, and Oke 1985, and references therein) and narrow-band imaging (A. Stockton, private communication) surveys of low-redshift quasars have demonstrated that the spatially resolvable structure around low-z QSOs can in some cases be significantly contaminated by strong extranuclear regions of emission-line gas. Our calculated host galaxy absolute magnitudes (§ II*b*[ii]) include all the light passing through our V-filter bandpass (lines plus continuum). To compare these absolute magnitudes to those of normal galaxies (which do *not* generally have very strong extranuclear emission lines, Kennicutt and Kent 1984), we would ideally need to remove the line contribution using detailed two-dimensional spectrophotometry of the fuzz around each of our QSOs. We can use Boroson *et al.*'s data for this purpose for the objects 0049+171, 2130+099, 2141+175, 2209+185, and 2251+113, which are common to our programs. For our other QSOs, we have used Boroson *et al.*'s data on 24 QSOs to calculate the median value of the equivalent width of the [O III] λ5007 emission line in low-redshift QSO fuzz. The procedure to decontaminate the fuzz is complicated by two factors. First, Boroson *et al.* find that radio-loud QSOs with steep-spectrum (large-scale double) radio sources generally have strong extranuclear line emission, while radio-quiet QSOs and QSOs with compact, flat-spectrum radio emission generally do not. We have therefore classified our QSOs into these three bins. We take a radio spectral index of $\alpha = 0.5$ at a frequency of $\sim$1.4 GHz ($S_\nu \propto \nu^{-\alpha}$) as the dividing point between steep and flat-spectrum radio-loud QSOs (radio data from Véron-Cetty and Véron 1984; Kühr *et al.* 1979; Dixon 1970). We will discuss our criterion for distinguishing radio-loud from radio-quiet QSOs in more detail in § III. For the three classes (quiet, steep, flat), we find median [O III] λ5007 equivalent widths of 12, 290, and 20 Å respectively. We take the respective equivalent widths of [O III] λ4959 and Hβ to be 0.33 and 0.17 of the above values.

Second, the degree to which these three emission lines will contaminate our V-band images will be a moderately strong function of QSO redshift (other emission lines are of negligible strength in the V filter for our sample's range of QSO redshifts). Thus, we have explicitly taken the transmissivity of the V filter as a function of wavelength into account in determining the likely fraction of "fuzz" light which is due to emission lines. The corrected (emission-line free) and averaged (from the two independent analyses) absolute magnitudes of the host galaxies are listed in Table 2. Owing to the statistical nature of these corrections, corrected magnitudes for individual galaxies may be over- or underestimated, but the sample as a whole should be properly corrected. In any case, the corrections are relatively small (0–0.5 mag with an average of only 0.1 mag), so errors in this procedure should not have important effects on our subsequent analysis.

III. RESULTS

The results of our image analysis are summarized in Table 2, and comments concerning individual objects may be found in the Appendix.

a) Comparisons to Other Imaging Surveys

We have compared our values for the absolute blue magnitudes of the host galaxies M_B^{GAL} (Table 2, third from last col.) to values derived by other groups for the 25 measurements of the 15 QSOs in common (Malkan 1984; MMC; Wyckoff, Wehinger, and Gehren 1981; Gehren *et al.* 1984; HCC; Boroson, Oke, and Green 1982; Boroson, Persson, and Oke 1985; Boroson and Oke 1984). We have converted all magnitudes to an $H_0 = 100$ km s^{-1} Mpc^{-1}, $q_0 = 0$ cosmology. When available (for 13 hosts), we have used blue magnitudes from the other imaging surveys. Otherwise, we have converted to B, assuming $B-V = 0.7$ and $B-r \approx 1.1$ for the hosts (in the QSO frame). We then find an average disagreement in M_B^{GAL} of $\sim$0.7 mag (our hosts are, on average, 0.5 ± 0.2 mag brighter).

To explore the possible causes for this disagreement in more detail, we have compared values of M_B^{GAL} not only between our survey and others but among the other surveys. We then find that comparisons between surveys based on linear, digital detectors (CCDs and SIT Vidicons) yield significantly better agreement than comparisons involving surveys based on photographic data. The mean difference in M_B^{GAL} is only 0.6 mag for the 24 cases in which "linear" data are compared with other such data but is 1.3 mag for the 35 cases in which photographic data are compared with linear data or other photographic data.

This result agrees with the contention of Gehren *et al.* (1984) and Bendinelli *et al.* (1984) that large (and systematic) errors in derived galaxy properties are difficult to avoid using photographic data. For this reason, we will use only data acquired with linear detectors in our quantitative consideration of QSO host properties below. However, for morphological/qualitative questions we will make use of all the available imaging data.

b) Classification of QSO/AGNs

It has become increasingly clear that there exists a broad continuity in properties between active galactic nuclei (AGNs) and QSOs. The question then naturally arises as to whether it is useful (or meaningful) to define a boundary between the two classes. From the standpoint of the present paper we think the answer is a qualified yes. It is quite possible that the properties of the host galaxies of QSOs are systematically different from those of mere AGNs. This might either reflect the effect of the nuclear activity on the host or be related to the processes by which very luminous nuclear activity is engendered.

Motivated by these considerations, two possible criteria for differentiating between QSOs and AGNs might be employed, depending on whether the luminosity of the nucleus or instead the luminosity of nucleus relative to luminosity of the host galaxy is likely to be the most physically important parameter. A plausible case could be made for either situation, so we will classify the objects in our sample (and when relevant from the literature) according to both a luminosity and "morphological" L_{PT}/L_{GAL} criterion (see also Bothun *et al.* 1984).

In the second column of Table 2 we classify objects with $L_{PT}/L_{GAL} > 1$ to be "quasi-stellar" in appearance, and denote them by "Q". Objects with $L_{PT}/L_{GAL} < 1$ are denoted by "G," since galaxy light is presumed to dominate their images. We then follow Schmidt and Green (1983) by choosing $M_B = -21.5$ (for $H_0 = 100$, $q_0 = 0$) as the luminosity boundary between high-luminosity QSOs and low-luminosity QSO/AGNs. Note that this criterion applies only to the fraction of the light coming from the active nucleus itself, excluding all

galaxy light. High-luminosity QSOs with $M_B \leq -21.5$ are denoted by "H," while lower luminosity QSO/AGNs are denoted by "L."

Since we will consider below many of the properties of QSO and AGN host galaxies according to whether or not the QSO or AGN is radio-loud, we have also adopted a rigorous definition of this term. Specifically, we will call an AGN or QSO "radio loud" if the quantity $\alpha_R^O \geq 0.4$. Here α_R^O is the effective optical-to-radio spectral index:

$$\alpha_R^O \equiv \frac{\log (S_{\nu O}/S_{\nu R})}{\log (\nu_O/\nu_R)} ,$$

where $S_{\nu O}$ and $S_{\nu R}$ are the flux densities at $\nu = 6.7 \times 10^{14}$ Hz and $\nu_R = 1.4 \times 10^9$ Hz (ν in the QSO or AGN rest frame). Note that $S_{\nu O}$ is as measured for the QSO or AGN alone (no galaxy contribution), and that $S_{\nu R}$ is the total radio flux density. We take a value of $\alpha_R^O = 0.4$ as the dividing line, since the fraction of optically selected QSOs falls off steeply as a function of α_R^O above this value (H. Marshall, private communication).

c) Host Absolute Magnitudes

In Figure 3*a* we display in histogram form the emission line–free absolute magnitudes for our sample of 31 host galaxies. Similarly, Figure 3*b* has been expanded to include the 58 other linearly imaged QSO and QSO/AGN host galaxies from the literature (Malkan 1984; MMC; Gehren *et al.* 1984; Boroson, Oke, and Green 1982; Boroson, Persson, and Oke 1985; Boroson and Oke 1984). These absolute blue magnitudes have been corrected for contamination by emission lines in the same way as our images and (if necessary) converted to B, assuming $B-V = 0.7$ and $B-r = 1.1$ for the host (see § II). These "corrected" magnitudes are listed in Table 3, along with the absolute blue magnitude of the QSO or QSO/AGN alone (computed from the literature values and converted to a rest-frame B magnitude, assuming that $B=V=R$). In cases where authors presented both a disk and an elliptical model, we naively chose to use the parameters derived for disk host galaxy when the QSO was radio quiet and for an elliptical host galaxy when the QSO was radio loud (based on the radio classification procedure outlined in § III*b*). Finally, Figure 3*c* displays a histogram of $M_B^{\rm GAL}$ for the 52 objects from Figure 3*b*

TABLE 3

RESULTS FROM OTHER QSO DIGITAL IMAGING AND SPECTROSCOPY STUDIES

Object	Class	M_B(host galaxy)[a]	M_B(point source)[b]
Boroson and Oke 1984[c]			
0134+32	QHl	−22.7	−24.4
1425+26	QHl	−21.8	−24.9
2201+31	QHl	−21.3	−24.5
Boroson *et al.* 1982			
0007+10	QLq	−20.0	−21.2
0052+25	QHq	−20.4	−22.1
1501+10	QLq	−19.7	−20.6
1519+22	QLq	−19.7	−20.3
1535+54	QLq	−19.4	−20.6
1612+26	QHq	−20.0	−21.5
1613+65	GLq	−21.9	−21.4
1617+17	QLq	−19.9	−21.3
1626+55	GHq	−21.6	−20.9
Boroson *et al.*1985[c]			
0953+41	QHq	−20.4	−25.0
1100+77	QHl	−21.0	−24.3
1116+21	QHq	−20.7	−23.5
1202+28	QHl	−20.4	−23.0
1226+02	QHl	−20.4	−25.7
Data from Gehren *et al.* 1984			
0003+158	QHl	> −22.9	−25.5
0043+388	QLq	−17.3	−19.1
0054+144	QHl	−20.2	−22.2
0134+329	QHl	−22.0	−23.5
0154+316	QLl	−20.3	−21.1
0214+108	QHl	−21.1	−23.3
0241+622	QHl	−20.8	−21.5
1257+286	GLq	−19.0	−18.9
2201+315	QHl	−22.2	−23.7
2214+350	QHl	−21.0	−22.3
2308+098	QHl	−21.5	−23.9
Data from Malkan *et al.* 1984			
0100+021	QHq	−20.8	−22.5
0120+091	QLq	−19.6	−21.4
0318+196	QHq	−19.7	−21.7
0351+026	GLq	−17.8	−17.8
0844+377	QHq	≥ −21.5	−23.2
1059+730	QLq	−19.5	−20.7
1339+053	QHq	−20.7	−22.2
1351+695	QHq	−20.1	−22.8
1403+546	QLq	−18.0	−19.8
1440+356	QHq	−20.4	−22.1
1519+279	QHq	−18.6	−22.1
1526+286	QHq	−22.2	−23.5
1534+580	QLq	−19.7	−19.8
1557+272	QLq	−17.8	−18.4
1613+658	QHq	−21.5	−23.0
1701+610	QLq	−20.2	−21.0
1704+607	QLq	−17.7	−20.1
2344+184	QLq	−19.8	−20.9
Data from Malkan 1984			
0134+329	QHl	−22.2	−23.5
1128+315	QHl	−21.7	−23.3
1150+497	QHl	−20.8	−21.9
1250+569	QHl	−20.5	−20.9
1304+346	QHq	−20.0	−22.4
1306+352	QHl	≥ −19.0	−21.4
1351+267	QHl	−20.7	−21.6
1425+267	QHl	−22.1	−23.0
1525+227	QHl	−20.2	−21.9
1546+027	QHl	−22.0	−22.6
1606+180	QHl	−21.2	−21.9
1612+266	QHq	−21.3	−23.7
1635+119	QHl	−20.9	−21.5
1720+246	QHl	−21.3	−22.3
1727+502	QLq	−19.5	−20.1
1745+163	QHl	≥ −20.9	−23.3
2140+548	QHl	−21.6	−22.0

[a] Host galaxy absolute blue magnitude corrected to $H_0 = 100\,{\rm km\,s^{-1}\,Mpc^{-1}}$, $q_0 = 0$, and emission lines removed.
[b] Nuclear point source absolute blue magnitude.
[c] Last column gives point source plus host galaxy magnitude. Isolated point source magnitude not determined. Difference should be negligible.

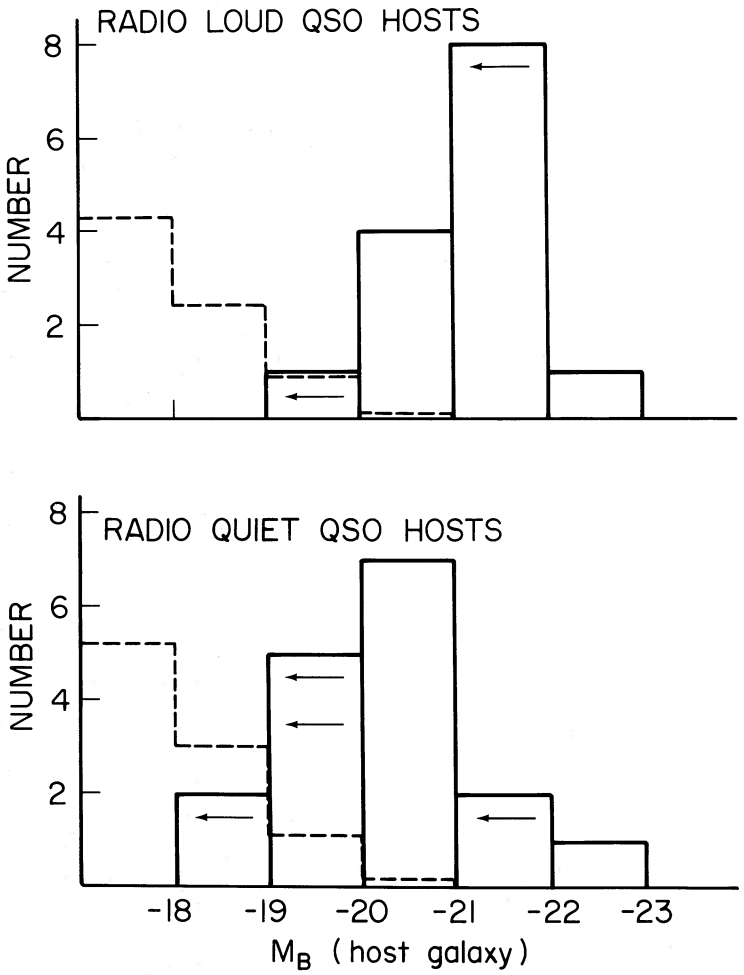

FIG. 3a

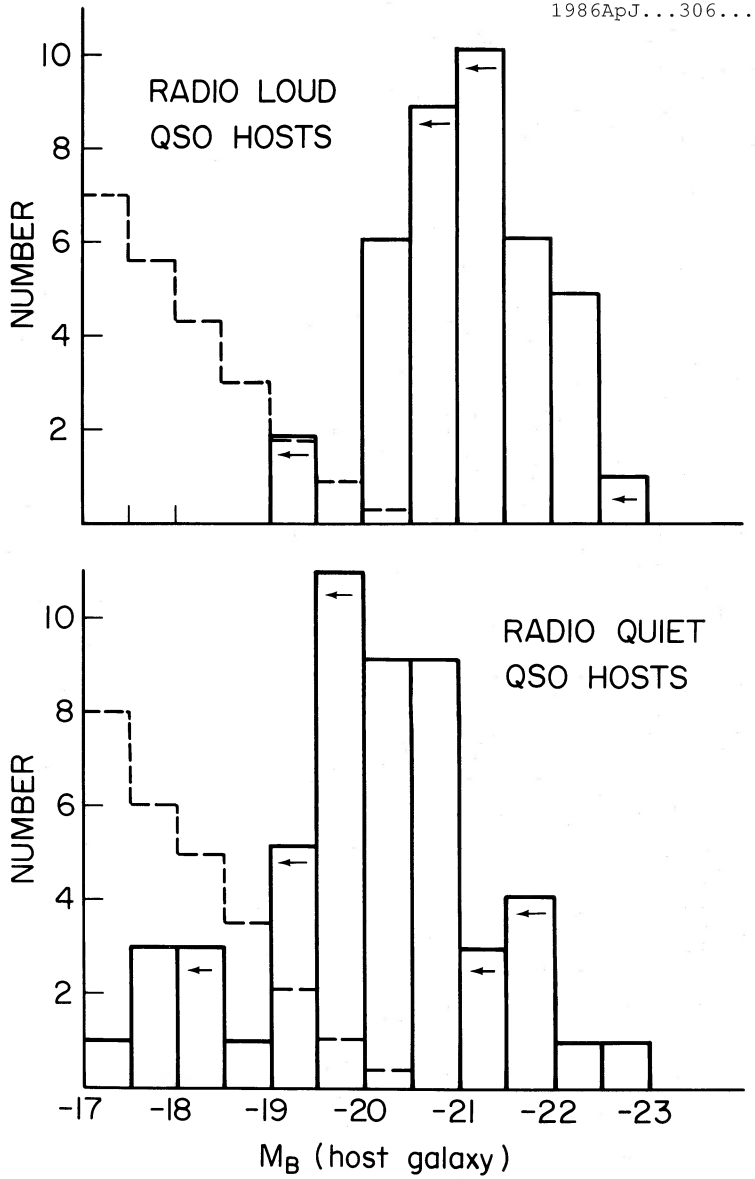

FIG. 3b

FIG. 3.—(*a*) Distribution of host galaxy absolute blue magnitudes ($H_0 = 100$, $q_0 = 0$, emission lines removed) for our sample. Arrows indicate upper limit for unresolved or marginally resolved host galaxies. Dashed line represents approximate expected distribution of normal galaxies that follows the Schechter luminosity function. (*b*) Distribution of host galaxy absolute blue magnitudes for data from this paper; Malkan (1984); MMC; Gehren *et al.* (1984); Boroson and Oke (1984); Boroson, Oke, and Green (1982); and Boroson, Persson, and Oke (1985).

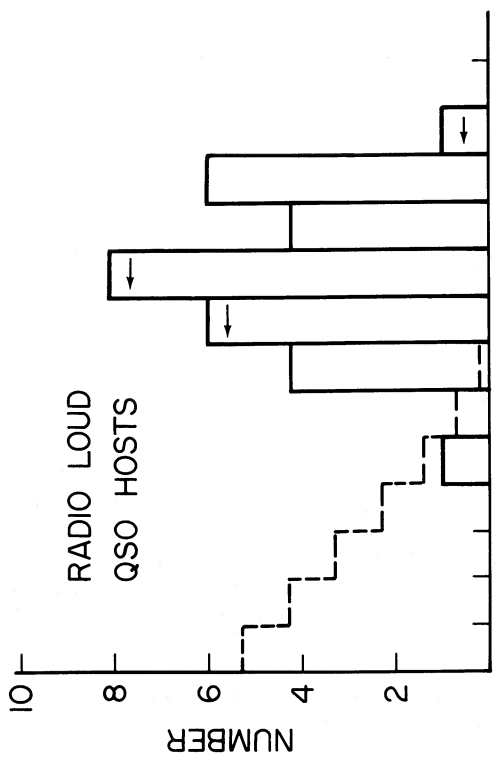

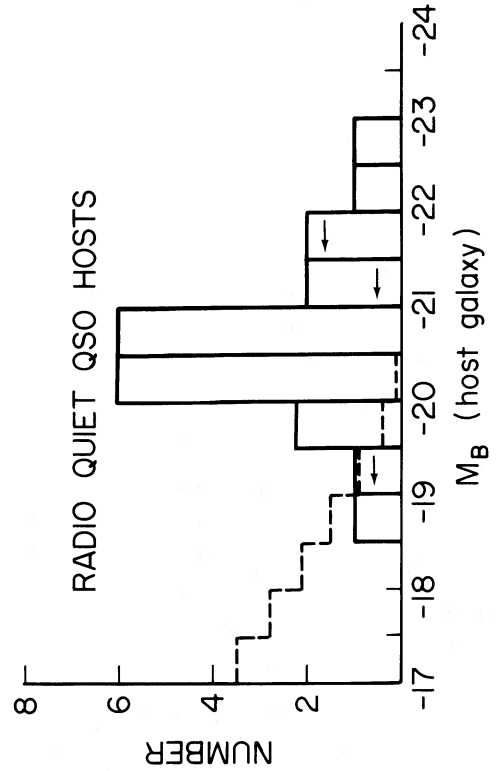

Fig. 3c

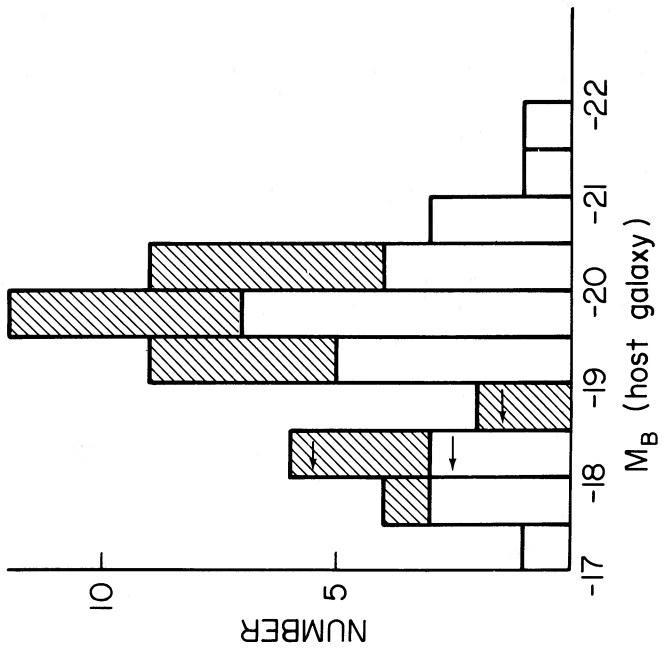

FIG. 4

FIG. 3c.—Distribution of host galaxy absolute blue magnitudes for data from Fig. 3b for objects with M_B(point source) ≤ -21.5

FIG. 4.—Distribution of host galaxy magnitudes for those objects not meeting Schmidt-Green QSO criteria along with Seyfert host galaxy data from Yee (1983). Shading indicates Seyfert hosts.

TABLE 4

MEAN ABSOLUTE MAGNITUDES

Sample[a]	Number	$\langle M_B \rangle$[b]	Significance[c]
Fig. 3*a*, l	14	-21.07 ± 0.22	~99.5%
Fig. 3*a*, q	17	-19.99 ± 0.31	
Fig. 3*b*, l	39	-21.01 ± 0.13	>99.9%
Fig. 3*b*, q	51	-19.85 ± 0.17	
Fig. 3*c*, l	30	-21.11 ± 0.14	~99.5%
Fig. 3*c*, q	22	-20.35 ± 0.22	
Fig. 4, q	28	-19.43 ± 0.22	~18%
Fig. 4[d]	20	-19.35 ± 0.20	

[a] Sample consists of radio-loud (l) or radio-quiet (q) QSOs and QSO/AGN hosts portrayed in the named figure, except for the last row.

[b] Mean absolute blue magnitude and dispersion of sample, taking into account upper limits on appropriate host galaxy magnitudes via the methods outlined in Feigelson and Nelson 1985 and Schmitt 1985.

[c] Logrank test values for level of significance of difference between the two populations.

[d] Seyfert hosts only.

that meet the Schmidt and Green (1983) QSO luminosity criterion $M_B \leq -21.5$. In Table 4 we list the mean values for $M_B^{\rm GAL}$ for the various host galaxy samples. Several interesting conclusions can be drawn from these figures:

1. In each of Figures 3*a*–3*c* we have also over-plotted the form of the Schecter luminosity function, to emphasize that *the QSO host galaxies are not drawn randomly from the population of galaxies as a whole, but are instead generally drawn from the high-luminosity "exponential tail" of the luminosity function.* Given the agreement in derived values of $M_B^{\rm GAL}$ among the various linear imaging surveys (average discrepancy, ~0.6 mag) and the excellent agreement between the values for $M_B^{\rm GAL}$ computed by two independent techniques (§ II), the observational basis for this statement is quite secure. Moreover, the effect on Figure 3 of the unresolved objects (which could possibly be low-luminosity host galaxies) will be minimal, since such objects comprise only ~10% of the samples.

To evaluate the possible impact of selection effects on the above conclusion, it is most illuminating to concentrate on Figure 3*c* concerning the hosts of luminous QSOs ($M_B \leq -21.5$). The QSOs in Figure 3*c* were generally discovered as strong radio sources, X-ray sources, or compact UV-excess objects in objective prism surveys. All these discovery techniques are independent of the prominence of the underlying galaxy (especially since the average value for $L_{\rm PT}/L_{\rm GAL}$ for the objects in Fig. 3*c* is $\gtrsim 6.7$). In fact, the only plausible selection effect which is relevant will work in the sense that QSOs hosted by exceptionally luminous galaxies might be preferentially *excluded* from catalogs of QSOs, since they would be more likely to appear slightly "fuzzy" on the POSS (or on other "discovery" images). We discuss the implications and interpretation of the preference of QSOs for luminous galaxies in § IV.

2. *The radio-loud host galaxies are typically a magnitude more luminous than the radio-quiet host galaxies.* This can be seen graphically in Figure 3 and in the appropriate sample parameters and statistical significances summarized in Table 4. This result is in agreement with Malkan (1984), HCC, and Gehren *et al.* (1984) and is also consistent with the belief that radio-loud QSOs are related to radio galaxies (often luminous ellipticals; e.g., Sandage 1972), while radio-quiet QSOs are related to Seyfert galaxies (less luminous disk galaxies; e.g., Yee 1983).

As discussed above, given the way in which the QSOs in Figure 3*c* were discovered, selection effects are very unlikely to play any role in the difference in the host galaxy absolute magnitudes between the radio-quiet and radio-loud QSO classes.

3. *The host galaxies of radio-quiet QSOs are more luminous on average than Seyfert galaxies.* In Figure 4 we show a histogram of the host $M_B^{\rm GAL}$ for the radio-quiet AGNs in Figure 3*b* which did not meet the QSO luminosity criterion. We have added to this figure the Markarian Seyferts imaged by Yee (1983). For both the Yee Seyfert sample and for the low-luminosity QSO/AGN sample, the median value of $M_B^{\rm GAL}$ is ~ -19.4, compared to -20.4 for the hosts of radio-quiet high-luminosity QSOs in Figure 3*c*. For the Seyfert galaxy sample, Yee argues that selection effects will tend to bias it toward *luminous* galaxies (since the Markarian survey is a magnitude-limited survey, and the nuclei of Seyferts do not generally dominate the galaxy light). Thus, correction for this selection effect in the Seyfert sample would *enhance* the difference between the luminosity of Seyfert versus radio-quiet QSO hosts.

HCC and Gehren *et al.* (1984) have claimed that the QSO luminosity and the host luminosity are proportional to one another, but this conclusion has been questioned by Malkan (1984) on the grounds that objects consisting of low-luminosity QSOs hosted by luminous galaxies are excluded from consideration by HCC and Gehren *et al.* since they do not enter QSO catalogs (they are instead classified as Seyferts). We share Malkan's reservations and doubt that a strict proportionality between $L_{\rm PT}$ and $L_{\rm GAL}$ exists. Figure 5 shows the weak relationship between M_V(point source) and M_V(host galaxy) for objects in our sample. However, the fact that hosts of radio-quiet QSOs are, on average, ~1 mag luminous than Markarian Seyfert galaxies implies that some (complex) relationship does exist between the luminosity function of AGNs and the luminosity of the host galaxy (see Auriemma *et al.* 1977 for a discussion of an analogous problem for radio galaxies).

4. *The host galaxies associated with steep-spectrum, extended radio sources have the same average luminosity as those associated with flat-spectrum, compact radio sources.* In contrast, Boroson and Oke (1984) found strong systematic differences in the *spectroscopic* properties of the hosts in these two radio classes: the hosts in the former class were blue and exhibited strong spatially extended emission-line nebulosity, while those in the latter class were red and had weak spatially extended emission-line gas (see also Boroson, Persson, and Oke 1985). Further comparison of the natures of the hosts in these two classes is of particular interest in the context of "unified" models of extragalactic radio sources in which the compact radio sources are simply extended sources seen along the axis of the relativistic jets (e.g., Orr and Browne 1982).

d) Disk versus Elliptical Host Galaxies

One of the most interesting issues in QSO research concerns whether the difference between radio-loud and radio-quiet QSOs is strongly related to the Hubble type of the host galaxy (as appears to be the case for Seyfert versus radio galaxies). We have been able to obtain rough Hubble types (E vs. disk) for 12 of the 31 host galaxies modeled (10 radio quiet and only two

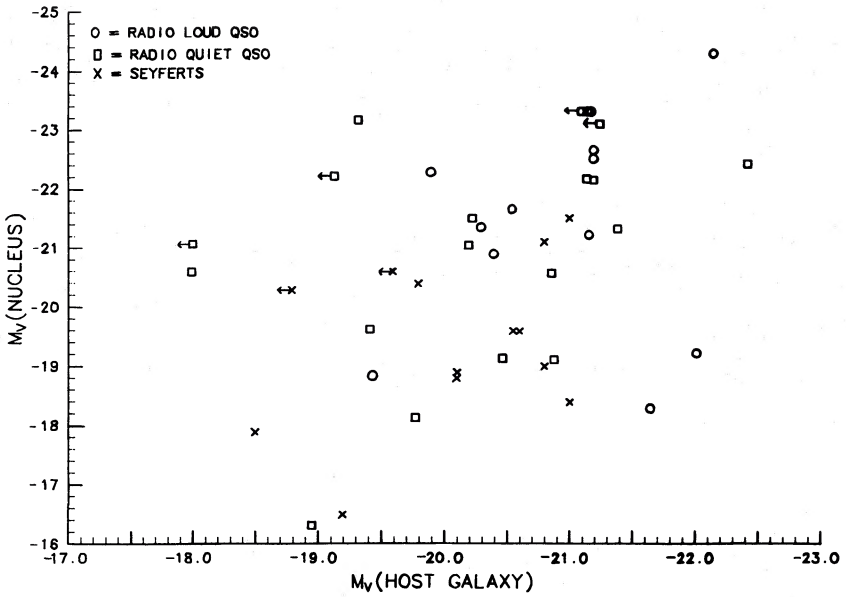

FIG. 5.—Host galaxy absolute V magnitudes (arrows indicate upper limits) vs. nuclear point source absolute V magnitudes data from this paper. Seyfert nucleus and host galaxy data from Yee (1983) included for comparison.

radio loud). By this we mean that for each of these 12 hosts, either an elliptical or disk model could be excluded at the 95% confidence level, while the other model could produce an acceptable fit with reasonable galaxy parameters. Of these 12 hosts, only one (the radio-quiet object 2209+185) did not conform to the pattern of disk galaxies being radio quiet and ellipticals being radio loud. Only four of these 12 objects have active nuclei which meet the Schmidt and Green QSO luminosity criterion. Of these, all three radio-quiet QSOs are apparently hosted by disk galaxies, and the only radio-loud QSO is hosted by an elliptical. These trends agree with the conclusions of MMC and Malkan (1984), which were based on a larger sample.

e) Morphologically Distorted Hosts

We find (in agreement with HCC) that the morphologies of many of the host galaxies in our imaged sample are markedly peculiar. Specifically, 35% (11 of 31) of the hosts display significant departures from an "elliptical" symmetry at higher surface brightness levels than $25V$ mag arcsec^{-2} above the sky ("distorted" hosts). Less rigorously, another $\sim$20% (six of 31) of the hosts exhibit some evidence at lower levels of surface brightness for asymmetric morphology ("possibly distorted").

There is no evidence for a higher degree of incidence of distorted or possibly distorted hosts among the luminous QSOs ($M_V \leq -21.5$) versus the low-luminosity QSO/AGNs. However (as found by HCC), the radio-loud hosts may be more frequently distorted or possibly distorted than the radio-quiet hosts: 10 of the 13 radio-loud hosts appear distorted or possibly distorted, versus only seven of the 18 radio-quiet hosts. These two populations differ at the 96% confidence level, according to a standard χ^2 "contingency table" test. Heckman *et al.* (1986) have found that many powerful radio *galaxies* are also morphologically peculiar.

IV. IMPLICATIONS OF THE HIGH LUMINOSITY OF QSO HOSTS

a) The Evidence

Of the various conclusions described in § III, the best established (and perhaps the most important) is that the host galaxies of luminous QSOs (radio loud or quiet) are not drawn randomly from the population of galaxies as a whole but are instead generally members of the rare class of galaxy that populates the exponential of the galaxy luminosity function. Before discussing the interpretation of this result, we demonstrate the strength of the supporting evidence.

First, this result is not based solely on our new imaging data but is also evident in all other major imaging and long-slit spectroscopic surveys of the properties of low-z QSO hosts done with linear detectors (Malkan 1984; MMC; Gehren *et al.* 1984; Boroson, Oke, and Green 1982; Boroson, Persson, and Oke 1985; Boroson and Oke 1984), as well as in the large photographic imaging survey discussed by HCC. Only the Lick spectroscopic survey of Miller (1981) is in possible conflict with this result. We discuss the implications of Miller's results in § IV*c*(ii[2]).

Second, we have carefully considered whether selection effects are responsible for the apparent preference of QSOs for luminous hosts, but given the facts that the QSOs were selected on the basis of their *nuclear* luminosities and that the QSOs optically dominate their hosts ($L_{PT}/L_{GAL} \approx 7$ on average), we believe it is unlikely that significant selection effects are present. Moreover, it is important to note that only $\sim$10% of the QSOs at $z < 0.5$ investigated with linear detectors are unresolved. Even if all these QSOs are hosted by dwarf galaxies, the strong preference for luminous hosts would be intact.

Finally, we emphasize that the high luminosities of the QSO host galaxies arise from starlight (or at least from continuum-emitting material), since we have statistically corrected the derived galaxy luminosities for the effect of spatially resolved emission-line nebulosities (using the extensive set of long-slit CCD spectra collected by Boroson and collaborators).

b) The Probability of a Galaxy Hosting a QSO

We have taken the distribution of the host galaxy absolute blue magnitudes (M_B^{GAL}) from Figure 3*c*, the Schechter luminosity function for galaxies averaged over clusters and the field (Felten 1977), and the present-epoch QSO luminosity function

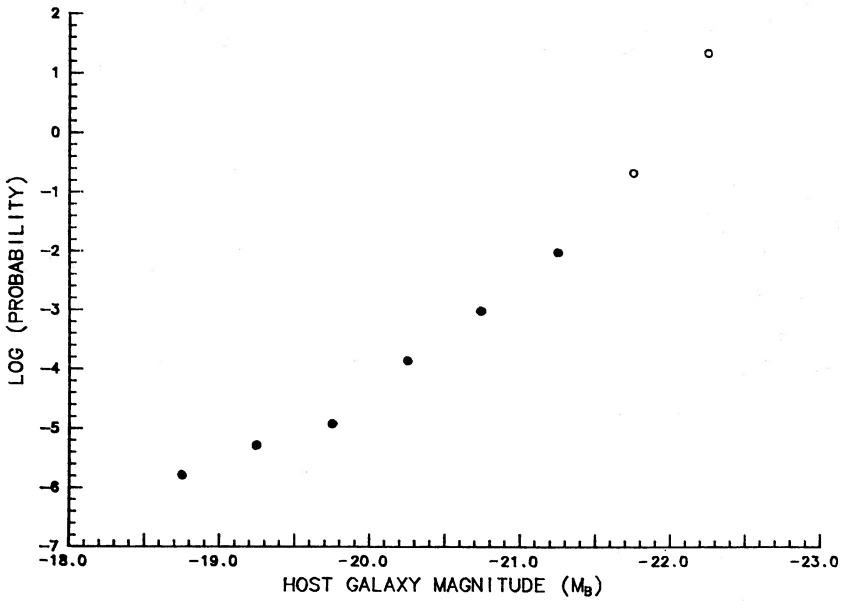

FIG. 6.—Absolute probability of a galaxy of magnitude M_B hosting a QSO or AGN, assuming that prior to the QSO's "turn-on" the host galaxies follow the distribution in M_B displayed in Fig. 3*c*. Normalization of absolute probability comes from the luminosity functions of Felten (1977) and Schmidt and Green (1983) for galaxies and QSOs respectively. Open circles represent an extrapolation of the analytic form of the Schechter-type galaxy luminosity function into a region where few data exist for normal galaxies. See text for more detail.

of Schmidt and Green (1983) to construct Figure 6, which represents the absolute probability of a galaxy hosting a QSO ($M_B \leq -21.5$) as a function of $M_B^{\rm GAL}$ at the present epoch. The procedure used was as follows. The QSO luminosity function gives the total space density of QSOs, which, used in conjunction with the distribution of $M_B^{\rm GAL}$ in Figure 3*c*, gives the space density of QSO host galaxies per half-magnitude bin in $M_B^{\rm GAL}$. Dividing this by a similarly binned version of the total galaxy luminosity function yields Figure 6.

The very steep rise in the probability of hosting a QSO as $M_B^{\rm GAL}$ becomes more negative is essentially the inverse in the exponential drop in the total galaxy luminosity function (since the distribution of $M_B^{\rm GAL}$ for the QSO hosts in Fig. 3*c* is relatively flat, between -20.0 and -22.5). The probabilities associated with two highest luminosity bins ($M_B^{\rm GAL} \leq -21.5$) are not to be taken seriously, since the luminosity function for galaxies is essentially undetermined in this range (e.g., Davis and Huchra 1982), and an extrapolation of the standard Schechter-style luminosity function was *assumed* in Figure 6. We emphasize that *Figure 6 is quantitatively meaningful only if the optical luminosity of the QSO host is not boosted by processes associated with the QSO or the QSO "turn on"* (see § IV*c*[ii]).

It is intriguing that the fraction of QSOs that are radio loud ($\sim$6% by our definition) is similar to the fraction of galaxies (averaged over the field and cluster) that are ellipticals ($\sim$10% from Davis and Huchra 1982 and Postman and Geller 1984). This implies that, if radio-loud QSOs are associated with elliptical galaxies and radio-quiet QSOs with disk galaxies, as the evidence in § III*d* suggests, then the probability of an elliptical galaxy of a given absolute magnitude hosting a radio-loud QSO is roughly the same as the probability of a similarly luminous spiral galaxy hosting a radio-quiet QSO. The tendency for radio-loud QSO hosts to be somewhat more luminous than radio-quiet QSO hosts might then reflect the higher luminosity of the fiducial L_* in the Schechter luminosity function for ellipticals versus disk galaxies (e.g., Tammann, Yahil, and Sandage 1979; Sebok 1982). Better data on QSO hosts and on the normal galaxy luminosity functions at the high-luminosity end are needed to test these ideas more quantitatively.

c) Interpretation

The preferential association of QSOs with luminous host galaxies can be interpreted in two ways, depending on the direction of the causal connection underlying the association. First, optically luminous galaxies may be particularly well suited to the production of a QSO (either because they are more likely to contain nuclear "engines" of the requisite mass, or because they are especially adept at fueling this engine). This interpretation can be quantified as in Figure 6. Second, a burst of star formation ignited by the QSO (or by the processes that turned the QSO on) may have dramatically boosted the luminosity of the host galaxy.

i) *QSO Evolution and "Dead" QSOs*

If the first interpretation is correct, it has interesting implications for theories of the QSO central engine and places important constraints on QSO evolution models. In particular, pure density evolution models for QSOs cannot work if the present-epoch predilection of QSOs for luminous hosts seen in Figure 3*c* was as strong at high redshift (the number of suitable hosts being a very small fraction of all galaxies; see Fig. 6).

Figures 3*c* and 6 also suggest that the nuclei of highly luminous galaxies are the most likely sites for "dead QSOs" (i.e., a massive central engine presently in a dormant state). More quantitatively, Phinney (1983) has concluded that to produce the observed total amount of energy radiated by QSOs over the history of the universe, $\sim 10^7 \epsilon_{10\%}^{-1} M_\odot$ of "burnt" matter should exist on average in the core of each galaxy more luminous than a Schechter L_* galaxy. Here the efficiency with which energy is produced is $\epsilon_{10\%} \equiv 10 E_{\rm LUM}/M_{\rm CE} c^2$, where $E_{\rm LUM}$ is the

total amount of luminous energy radiated by a QSO over its entire lifetime and M_{CE} is the mass of the central engine. His estimate assumed that dead QSOs reside exclusively in galaxies with $L > L_*$, but that above L_* the probability of a galaxy of luminosity L having hosted a QSO [$P(L)$] is independent of L [taking $P(L) = 1$ for $L \geq L_*$ then gives the above estimate for the *average* value of M_{CE} per nucleus]. The distributions in Figures 3*c* and 6 suggest that a better assumption in the same spirit might be that $P(L) = 0$ for $L < L_*$, $P(L) \approx 1$ for $L \gtrsim 6L_*(M_B^{GAL} \leq -21.2)$, and $P(L) = 4.1 \times 10^{-4}(L/L_*) \exp(L/L_*)$ for $L = 1$–$6L_*$ [the latter equation being the inverse of galaxy luminosity function normalized so that $P(6L_*) = 1$]. In this case, the *average* value per galaxy nucleus for M_{CE} would be $\sim 10^9 \epsilon_{10\%}^{-1}\ M_\odot$ for galaxies brighter than $6L_*$, and $4.1 \times 10^5 (L/L_*) \exp(L/L_*) \epsilon_{10\%}^{-1}\ M_\odot$ for galaxies with $L = 1$ to $6L_*$.

ii) *QSO–induced Starbursts?*

As noted above, the high luminosity of QSO host galaxies may be due (at least in part) to a boosting of the host luminosity by a burst of star formation ignited by the QSO or by the processes which turned the QSO on (e.g., a galaxy collision), or both. In this case, Figure 6 and the above arguments concerning M_{CE} as a function of L would have little quantitative meaning. There are several pieces of evidence that support this hypothesis.

1. Long-slit spectroscopy is available for six of the 11 most luminous ($M_B \leq -21.5$) host galaxies in Figure 3*c* (Boroson and Oke 1984; Boroson, Oke, and Green 1982; Boroson, Persson, and Oke 1985; MacKenty and Stockton 1984; Heckman *et al.* 1984). In two cases (0134+329 and 0157+001), this host is very blue and its spectrum shows strong Balmer absorption lines. In two other cases (1425+267 and 2251+113), the host galaxy is blue and its spectrum shows strong emission lines. The Mg I *b* absorption line (a strong feature in the spectra of old evolved stellar populations) is abnormally weak (absent) in the spectrum of 1613+650. Only in the case of 2201+315 does the host spectrum appear consistent with that expected for a normal elliptical galaxy. These data suggest that the host galaxies of QSOs may not generally have "normal" (cool, old) stellar populations.

2. Miller (1981) has estimated upper limits to the luminosities of QSO host galaxies based on his failure to detect the Mg I *b* absorption line in the nuclear spectra of QSOs. These limits are generally lower (by typically ~ 1 mag) than the estimates of host luminosities derived from modeling of digital imaging or long-slit spectroscopic data in Table 3 for the six cases in common. This conflict can be reconciled if the Mg I *b* line is in fact significantly weaker in the spectrum of the QSO hosts than in the spectrum of a typical elliptical galaxy. This would be the case if the host were undergoing a starburst.

3. Evidence implicating galaxy interactions in both the QSO and the starburst phenomenon continues to mount (Lonsdale, Persson, and Mathews 1984; HCC).

4. Begelman (1985) has recently investigated theoretically the impact of a QSO on the interstellar medium of its host galaxy and finds that a significant increase in the global star-forming rate is indeed plausible during the early stages of the QSO's life.

If the distribution of M_B^{GAL} seen in Figure 3*c* does reflect the effect of the QSO in its host, the QSO phenomenon could have important implications for galaxy evolution—particularly during the "QSO epoch" at large redshift.

V. CONCLUSIONS

1. The agreement between independent estimates of the absolute magnitude of QSO and QSO/AGN host galaxies (after correction for the contamination by emission-line nebulosity) is good when data acquired with linear detectors (CCD or SIT images or CCD long-slit spectra) are compared with other such data (average disagreement 0.6 mag). The agreement between photographic and other data is poorer (1.3 mag average disagreement).

2. The host galaxies of QSOs (active nuclei with $M_B \leq -21.5$ for $H_0 = 100$ km s^{-1}, $q_0 = 0$) are generally luminous systems populating the exponential tail of the galaxy luminosity function (median $M_B = -20.7$ vs. $M_B = -19.2$ for a Schechter L_* galaxy).

3. Seyfert galaxies (galaxies hosting radio-quiet active nuclei with $M_B > -21.5$) are apparently less luminous (by ~ 1 mag on average) than the hosts of radio-quiet QSOs (respective medians -19.4 vs. -20.4). Selection effects for the Seyferts (if present) will only increase this disparity.

4. The radio-loud QSO host galaxies are more luminous than the radio-quiet QSO hosts ($M_B = -21.1$ vs. -20.4). This is also true for radio versus Seyfert galaxies (e.g., Auriemma *et al.* 1977; Sandage 1972; Yee 1983; see also HCC; Gehren *et al.* 1984).

5. For the sample of QSOs and QSO/AGNs, there is a trend for the radio-loud hosts to be better fitted by elliptical galaxy models and for the radio-quiet hosts to be fitted by disk galaxies (see also MMC; Malkan 1984). This trend suggests that the dichotomy known to exist between Seyfert and radio galaxies (e.g., Adams 1977; Matthews, Morgan, and Schmidt 1964) extends to much higher levels of nuclear luminosity.

6. Conclusions (4) and (5) strengthen the empirical basis for a continuity in properties between Seyfert galaxies and radio-quiet QSOs and between radio galaxies and radio-loud QSOs.

7. At low levels of surface brightness, the host galaxies of QSOs and QSO/AGNs are often markedly distorted in morphology (with a fraction near one-half our sample, depending on the criteria used). There is also some indication that the radio-loud hosts are more likely to be morphologically peculiar than the radio-quiet hosts ($\sim\frac{3}{4}$ vs. $\sim\frac{1}{3}$ of the respective samples). These conclusions both agree with those drawn by HCC.

8. The strong predilection of QSOs for luminous host galaxies may imply that such hosts are much more likely to contain suitably massive central engines or are especially adept at fueling them or both. In this case, pure density evolution of the QSO population with cosmic time is unlikely. This interpretation would also suggest that the nuclei of very luminous galaxies ($M_B \leq -21.7$; $L \geq 10L_*$) are the best candidates for "dead QSOs" ($\sim 10^9\ M_\odot$ of "burnt" matter per nucleus?).

9. Alternatively or additionally, the high luminosity of QSO hosts may be caused in part by a global burst of star formation triggered by the QSO or by the processes which fuel the QSO or both. This hypothesis is consistent with available spectroscopic data on the QSO host galaxies and may have important implications for our understanding of galaxy evolution.

We would like to thank the staff of the Cerro Tololo Inter-American Observatory for their help. E. S. Thanks the Laboratory for Astronomy and Solar Physics at NASA/GSFC for its generous allocation of computing time. We would also like to thank referee Matt Malkan for helpful comments. T. H. and E. S. were supported by NSF grant AST82-16553.

APPENDIX

NOTES ON INDIVIDUAL OBJECTS

Following the object name is the type of galaxy model(s) that gave good fits to the observed profiles. Objects listed in Table 2 and not specifically discussed below can be characterized by circularly symmetric isophotes.

0031−076.—[Disk] Extended emission is evident to the southeast of the center. Inner isophotes are also elongated in this direction. This object meets neither our morphological nor luminosity criteria for QSOs and should not be properly considered a QSO. In the case of the two X-ray–selected objects, 0031−076 and 0037+061, good fits could be obtained by setting the scale of the PSF to zero. In practice this means that the ratio of L_x/L_{opt} for X-ray–selected objects is actually higher, since L_{opt} is determined from apture photometry, assuming that all the light comes from the the point source (cf. Margon, Downes, and Chanan 1985).

0037+061.—[Disk] Image is symmetric about the major axis. Faintest isophote has a $b/a = 0.69$ and p.a. = 40°. Although best fitted by a disk galaxy plus a point source, we find no direct evidence for spiral arms, contra HCC. Not a QSO by either a luminosity or a morphological criterion. See comments for object 0031−076.

0049+171.—[E and Disk] Disk fit is more reasonable, as E-model has a large r_e for its M_B compared to normal ellipticals.

0050+124 (I Zw 1).—[Disk] Object to north is a star, while object at west is a companion galaxy, as discussed by Heckman *et al.* (1984). Isophotes are very distorted at low levels. No evidence for true spiral arms, but a tightly wrapped armlike extension is seen in the northwest quadrant. Despite its low redshift, this object easily meets both the morphological and luminosity criteria for QSOs. H I λ = 21 cm emission detected by Bothun *et al.* (1984) and Condon, Hutchings, and Gower (1985).

0134+033.—[Disk] Low-level isophotes merge with a nearby galaxy, as noted by HCC. Some of the inner contours are eccentric, and a rotation of the isophotal major axis with radius is apparent. Morphologically it is a QSO, but the "QSO" luminosity is low.

0135−047.—[E and Disk] Disk fit yields unrealistically low central surface brightness for underlying galaxy. More likely an elliptical.

0137+012.—[E] Because of the proximity of the two blobs in the image, this QSO proved very difficult to model. We exclude the two blobs from the luminosity profile, leaving only a small portion (from p.a. = 180°–320°) suitable for analysis. Emission is slightly extended along the p.a. = 25° line. Meets neither the morphological nor luminosity criteria for QSOs.

0146+089.—[Disk and E] Elliptical fit gives small r_e for M_B compared to normal elliptical galaxies.

0157+001.—[Disk] This QSO provided one of the most interesting images in the survey. It was the only object to display significant isophotal twisting, with the p.a. ranging over ~180° in a radius of 20 pixels. The center of the object shows a strongly peaked source, while the outer isophotes strongly suggest the presence of an armlike feature to the northeast. This feature is probably not a normal spiral arm, as there is no corresponding feature on the other side of the image, and hence may be a tidally disrupted part of the galaxy. We obtained the best fit for an underlying galaxy with $b/a = 0.6$, p.a. = 100°. The brightness and size derived for this object are quite large for a spiral galaxy. It was by far the most luminous spiral in our survey and was shown by MacKenty and Stockton (1984) to have a young stellar population (see also Heckman *et al.* 1984). Meets both morphological and luminosity criteria for QSOs.

0213−484.—[Disk] Two nearby galaxies with projected distances less than 40 kpc from the QSO are evident in this image, as is the eccentricity of the QSO fuzz. Galaxy fits used model with $b/a = 0.6$, p.a. = 144°. Meets both morphological and luminosity criteria for QSOs.

0736+017.—[E and Disk] Object has an extended low surface brightness halo and very large effective radius. Disk fit yields unrealistically low central surface brightness for underlying galaxy. May be a cD galaxy.

2130+099 (II Zw 136).—[Disk] QSO host has isophotes of varying ellipticities. Strong central source produces circular contours, while underlying galaxy is responsible for eccentric isophotes. Luminosity profile was generated by using circularly averaged values for inner 10 pixels and elliptically averaged ($b/a = 0.5$, p.a. = 55°) values for outer part of picture. HCC note spiral arm features in blue exposure which do not show up in our V image. Despite its low redshift, this object meets both the morphological and luminosity criteria for QSOs.

2135−147.—[Disk and E] Companion galaxy enclosed within fainter isophotes. Easily meets luminosity and morphological criteria for a QSO. Disk model has low central surface brightness compared to normal disk galaxies.

2141+175.—[E and Disk] QSO displays jetlike feature 30 kpc in extent to the southeast of image, and smaller extensions are seen to the northwest and southwest (see Heckman *et al.* 1986 for more details). Difficult to model successfully. Luminosity profiles were calculated using $b/a = 0.8$. Image strongly peaked (and therefore circular) in center. Meets both morphological and luminosity criteria for QSOs.

2209+185.—[E] Circularly symmetric contours are slightly distorted toward nearby galaxy. Meets neither luminosity nor morphological criteria for QSOs.

2215−037.—[Disk and E] Galaxy to the north of QSO has a significantly different redshift (Heckman *et al.* 1984). A QSO on the basis of both luminosity and morphology.

2247+140.—[E and Disk] Difficult to model successfully. The fuzz to the southeast shows isophotal twisting, indicating the presence of an armlike feature. However, faint material stretching out ~20″–25″ to the northwest would be quite unusual for a normal spiral galaxy (see Heckman *et al.* 1986). Models used $b/a = 0.6$, p.a. = 115°. Meets both the morphological and luminosity criteria for QSOs.

2251+113.—[E] Asymmetry to the northwest in outer contours appears spurious. Attempts to obtain fits were only marginally successful ($\chi^2 \approx 1.9$), even excluding this quadrant of the image. A QSO by both morphology and luminosity. Model has small r_e for its M_B compared to normal ellipticals.

2300−189.—[E and Disk] A jetlike feature is evident to the southeast of the QSO. When obtaining the luminosity profile for this

object, we cut out the northwest quadrant of the image where a nearby companion galaxy is located (see Hunstead *et al.* 1984). Although there is marked asymmetry in the fainter portions of this image, the central brightness is quite concentrated and pointlike. This object is discussed in more detail by Heckman *et al.* (1986). It meets neither morphological nor luminosity criteria for QSOs. Extensive halo: asymptotic absolute magnitude is 0.8 mag brighter than the magnitude interior to R_{25}.

2304+043.—[Disk] Ellipticity of isophotes varies from $b/a = 0.5$ to $b/a = 0.8$ as one travels out from the center of the image. This may indicate an inner barlike structure. Meets neither morphological nor luminosity criteria for QSOs.

2305+187.—[E and Disk] Elliptical galaxy model is too bright for effective radius. Disk model yields more realistic parameters.

REFERENCES

Adams, T. F. 1977, *Ap. J. Suppl.*, **33**, 19.
Auriemma, C., Perola, G. C., Ekers, R., Fanti, R., Lari, C., Jaffe, W. J., and Ulrich, M. H. 1977, *Astr. Ap.*, **57**, 41.
Balick, B., and Heckman, T. M. 1983, *Ap. J. (Letters)*, **265**, L1.
Begelman, M. C. 1985, *Ap. J.*, **297**, 492.
Bendinelli, O., Lorenzutta, S., Parmeggiani, G., and Zavatti, F. 1984, *Astr. Ap.*, **138**, 337.
Boroson, T. A., and Oke, J. B. 1984, *Ap. J.*, **281**, 535.
Boroson, T. A., Oke, J. B., and Green, R. 1982, *Ap. J.*, **263**, 32.
Boroson, T. A., Persson, S. E., and Oke, J. B. 1985, *Ap. J.*, **293**, 120.
Bothun, G. B., Heckman, T. M., Schommer, R. A., and Balick, B. 1984, *A.J.*, **89**, 1293.
Bruzual, G. 1983*a*, *Rev. Mexicana Astr. Ap.*, **8**, 63.
———. 1983*b*, *Ap. J.*, **273**, 105.
Burstein, D. A., and Heiles, C. 1982, *A.J.*, **87**, 1165.
Condon, J. J., Hutchings, J. B., and Gower, A. C. 1985, *A.J.*, **90**, 1642.
Davis, M., and Huchra, J. 1982, *Ap. J.*, **254**, 437.
Dixon, R. S. 1970, *Ap. J. Suppl.*, **20**, 1.
Feigelson, E. D., and Nelson, P. I. 1985, *Ap. J.*, **293**, 192.
Felten, J. 1977, *A.J.*, **82**, 861.
Gehren, T., Fried, J., Wehinger, P. A., and Wyckoff, S. 1984, *Ap. J.*, **278**, 11.
Heckman, T. M., Bothun, G. D., Balick, B., and Smith, E. P. 1984, *A.J.*, **87**, 958.
Heckman, T. M., van Breugel, W. J. M., Balick, B., Miley, G. K., Bothun, G. D., Illingworth, G. D., Smith, E. P., and Baum, S. A. 1986, *Ap. J.*, submitted.
Hewitt, A., and Burbidge, G. 1980, *Ap. J. Suppl.*, **43**, 57.
Holmberg, E. 1975, in *Stars and Stellar Systems*, Vol. **9**, *Galaxies and the Universe*, ed. A. Sandage, M. Sandage, and J. Kristian (Chicago: University of Chicago Press), p. 123.
Hunstead, R. W., Murdoch, H. S., Condon, J. J., and Phillips, M. M. 1984, *M.N.R.A.S.*, **207**, 55.
Hutchings, J. B., Crampton, D., and Campbell, B. 1984, *Ap. J.*, **280**, 41 (HCC).
Kennicutt, R. C., and Kent, S. M. 1984, *Ap. J. (Letters)*, **279**, L5.
Kuhr, H., Nauber, U., Pauliny-Toth, I. I. K., and Witzel, A. 1979, *Catalog of Radio Sources* (Munich: Max Plank Institut für Radioastronomie).
Lonsdale, C. J., Persson, S. E., and Mathews, K. 1984, *Ap. J.*, **287**, 95.
MacKenty, J. W., and Stockton, A. 1984, *Ap. J.*, **283**, 64.
Malkan, M. 1984, *Ap. J.*, **287**, 555.
Malkan, M. A., Margon, B., and Chanan, G. A. 1984, *Ap. J.*, **280**, 66 (MMC).
Margon, B., Downes, R., and Chanan, G. 1985, preprint.
Matthews, T. A., Morgan, W. W., and Schmidt, M. 1964, *Ap. J.*, **140**, 35.
Miller, J. S. 1981, *Pub. A.S.P.*, **93**, 681.
Orr, M. J. L., and Browne, I. W. A. 1982, *M.N.R.A.S.*, **200**, 1067.
Pence, W. 1976, *Ap. J.*, **203**, 39.
Phinney, E. S. 1983, Ph.D. thesis, Cambridge University.
Postman, M., and Geller, M. J. 1984, *Ap. J.*, **281**, 95.
Romanishin, W., Ford, H., Ciardullo, R., and Margon, B. 1984, *Ap. J.*, **277**, 487.
Romanishin, W., and Hintzen, P. 1985, in preparation.
Rubin, V. 1983, in *IAU Symposium 100, Internal Kinematics and Dynamics of Galaxies*, ed. E. Athanassoula (Dordrecht: Reidel), p. 3.
Sandage, A. 1972, *Ap. J.*, **178**, 25.
Schmidt, M., and Green, R. 1983, *Ap. J.*, **269**, 352.
Schmitt, J. H. M. M. 1985, *Ap. J.*, **293**, 178.
Sebok, W. L. 1982, Ph.D. thesis, California Institute of Technology.
Stockton, A. 1982, *Ap. J.*, **257**, 33.
Stockton, A., and MacKenty, J. W. 1983, *Nature*, **305**, 678.
Tammann, G. A., Yahil, A., and Sandage, A. 1979, *Ap. J.*, **234**, 775.
Véron-Cetty, M. P., and Véron, P. 1984, *ESO Sci. Rept.*, **1**, 85.
Wyckoff, S., Wehinger, P. A., and Gehren, T. 1981, *Ap. J.*, **247**, 750.
Yee, H. K. C. 1983, *Ap. J.*, **272**, 473.
Yee, H. K. C., and Green, R. F. 1984, *Ap. J.*, **280**, 79.

B. Balick: Astronomy Department, FM-20, University of Washington, Seattle, WA 98195

G. D. Bothun: Astronomy Department, Mail Code 105-24, California Institute of Technology, Pasadena, CA 91125

T. M. Heckman and E. P. Smith: Astronomy Program, Space Science Building, University of Maryland, College Park, MD 20742

W. Romanishin: Department of Physics, Arizona State University, Tempe, AZ 85287